

Nodal liquid and s -wave superconductivity in transition metal dichalcogenides

B. Uchoa,¹ G. G. Cabrera,¹ and A. H. Castro Neto²

¹*Instituto de Física “Gleb Wataghin” Universidade Estadual de Campinas (UNICAMP), Caixa Postal 6165, Campinas, Sao Paulo 13083-970, Brazil*

²*Department of Physics, Boston University, 590 Commonwealth Avenue, Boston, Massachusetts 02215, USA*

(Received 17 September 2004; published 17 May 2005)

We explore the physical properties of a unified microscopic theory for the coexistence of superconductivity and charge-density waves (CDWs) in two-dimensional transition-metal dichalcogenides. In the case of particle-hole symmetry, the elementary particles are Dirac fermions at the nodes of the charge density wave gap. When particle-hole symmetry is broken, electron (hole) pockets are formed around the Fermi surface. The superconducting ground state emerges from the pairing of nodal quasiparticles mediated by acoustic phonons via a piezoelectric coupling. We calculate several properties in the s -wave superconducting phase, including specific heat, ultrasound absorption, nuclear magnetic relaxation (NMR), and thermal and optical conductivities. In the case with particle-hole symmetry, the specific-heat jump at the transition deviates strongly from ordinary superconductors. The NMR response shows an anomalous anisotropy due to the broken time-reversal symmetry of the superconducting gap, induced by the triple CDW state. The loss of the lattice inversion center in the CDW phase leads to anomalous coherence factors in the optical conductivity and to the appearance of an absorption edge at the optical gap energy. In addition, optical and thermal conductivities display anomalous peaks in the infrared when particle-hole symmetry is broken.

DOI: 10.1103/PhysRevB.71.184509

PACS number(s): 74.20.Mn, 71.10.Hf, 71.45.Lr

I. INTRODUCTION

The quasi-two-dimensional (2D) transition-metal dichalcogenides (TMD) 2H-TaSe₂, 2H-TaS₂, and 2H-NbSe₂ are layered compounds where s -wave superconductivity coexists with a charge-density wave (CDW)^{1,2} at low temperatures, and whose transport properties are highly anisotropic in the high temperature CDW phase.³ There is vast literature reporting anomalous effects in the CDW phase, including non-linear Hall effect, anomalous impurity effects in the superconducting (SC) phase,⁴ stripe phases,⁵ and different regimes of commensurability.⁶ Recent angle-resolved photoemission experiments (ARPES) reveal that the quasiparticles of the TaSe₂ crystal have a non-Fermi-liquid lifetime.⁷ This scenario becomes a little more exciting with the verification that some of the TMD properties, such as the linear growth of the normal resistivity with temperature,³ and the strong anisotropy in the in-plane and out-of-plane transport are similar to the same properties in the high-temperature superconductors (HTc). HTc do not show a CDW gap, but a d -wave *pseudogap* coexisting with the superconducting phase. In both cases, the transport and thermodynamic properties are weakly dependent on the application of external fields in the normal/pseudogap phase, and strongly dependent on them in the SC phase.⁸ Furthermore, the application of pressure in TMD favors the superconductivity in a broad range and suppresses the CDW phase,⁹ in close analogy with the HTc phase diagram temperature vs doping level. In contrast to the HTc, however, the TMD are very clean crystals. The anomalous TMD properties are sample independent and can help to clarify the physics behind a whole class of exotic low-dimensional superconductors.

The interpretation of the experimental data in TMD is, however, still very controversial. Within the Peierls theory, the CDW gap formation in 1D systems is usually due to

nested Fermi surfaces. In 2D systems, the nesting is not perfect and some parts of the Fermi surface may not be gaped. Early band structure calculations¹⁰ indicated that the Γ centered sheets (S_I) are nested with the K centered ones (S_{II}) by the \mathbf{Q}_i ($i=1,2,3$) wave vectors of the triple-CDW (see Fig. 1). The value of the CDW wave-vector, $|\mathbf{Q}_i| \sim \frac{1}{3}\Gamma K$, measured by neutron diffraction^{11,12} and some recent scanning-tunneling microscopy (STM) experiments^{13–15} confirm the plausibility of a nesting scenario. An alternative theory proposed by Rice and Scott¹⁶ is based in a Fermi-surface-independent CDW mechanism, where the CDW wave vectors connect the saddle points (indicated in Fig. 1, around $\frac{1}{2}\Gamma K$) of the transition metal d bands, generating a logarithmic divergence in the electronic susceptibility. However, the saddle-point energy in NbSe₂ is too large (~ 50 meV) in comparison to the CDW ordering thermal energy $k_B T_{CDW} \sim 3$ meV to allow a saddle-point driven instability.¹⁷ In TaSe₂, however, ARPES has observed an extended saddle band along ΓK . This band is nearly flat and closer to the Fermi energy than the band calculations predicted.^{18,19} As the saddle points are not well defined in this case, it is questionable to justify the CDW wave-vector measured with neutrons by some mechanism related to special parts of the saddle bands. More experimental studies are required to elucidate this point.

Although these arguments seem to rule out at least a conventional saddle-point mechanism, a consensus on the origin of the CDW instability has not been reached. STM scans at 4.2 K in TaSe₂, TaS₂, and NbSe₂ show that the amplitude of the CDW gap is $\Delta_{CDW} \sim 80, 50,$ and 34 meV, respectively.²⁰ The ability of ARPES to measure the SC gap $\Delta_s \sim 1$ meV $\ll \Delta_{CDW}$ in NbSe₂, combined with the complete failure of ARPES to detect traces of the CDW gap in the Brillouin zone of TaSe₂ and NbSe₂ (Refs. 7 and 21) were interpreted

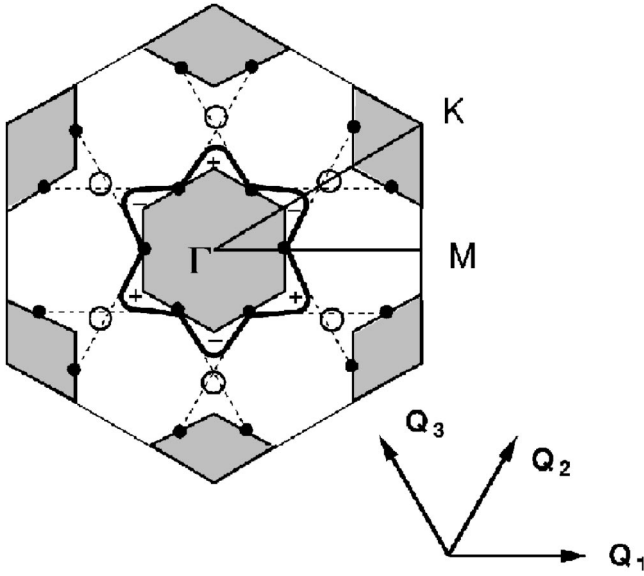


FIG. 1. Schematic representation of the TMD Fermi surface. The Γ centered sheet (S_I) is nested with the K centered ones (S_{II}) by the CDW wave vectors \mathbf{Q}_i . A CDW gap develops in the two sheets, except in the nodal points, indicated by the black filled circles. The empty circles are the saddle points. The thick solid line around the S_I sheet is the proposed CDW gap. The dashed lines indicate the nodes connected by \mathbf{Q}_i .

as an evidence that the Fermi surface is weakly covered by the CDW. We observe that the photoemission results seem to be in contradiction with the STM data, and cannot explain the non-Fermi-liquid transport in the TaSe₂ crystal. One possibility is that the ARPES data are obscured by the strong dependence of the CDW gap with the directions of the Brillouin zone combined with the formation of pockets in the points of the Fermi surface where $\Delta_c(\mathbf{k})=0$ ($\max[\Delta_c(\mathbf{k})]=\Delta_{\text{CDW}}$). Another possibility is that the ARPES electronic dipole matrix elements vanish for certain states in the CDW phase due to the broken spacial inversion symmetry (detected in neutron scattering)¹² forbidding the observation of some bands.

The strong resemblance of the normal CDW phase resistivity of TaSe₂ with the HTc²² and the anomalous quasiparticle lifetime decay, given by the inverse of the imaginary part of the electronic self-energy⁷ $\text{Im} \Sigma(k_F, \omega) \propto \tau_0^{-1} + b|\omega|$, indicates that a marginal Fermi liquid (MFL) theory²³ should be developed as the basis of a minimal model unifying the CDW and SC phases in TaSe₂. The experimental verification that $k_B T_{\text{CDW}} \ll \Delta_{\text{CDW}}$ for all the TMD crystals (in TaSe₂ for example, $k_B T_{\text{CDW}} \sim 120 \text{ K} = 12 \text{ meV}$) gives a good indication that a strong-coupling CDW theory is required.

One of us (A.H.C.N.)²⁴ has recently proposed a unified picture for the CDW and SC phases where the elementary particles are Dirac fermions that are created in the region where the CDW gap vanishes, leading to the generation of a nodal liquid. According to neutron-diffraction studies, the inversion center of the crystal is lost in the CDW phase,¹² allowing for the possibility of piezoelectric effects. In a system with nodal quasiparticles, the piezoelectric coupling is a marginal coupling from the renormalization group (RG)

point of view, while the usual electron-phonon coupling is irrelevant under the RG.²⁵ Based on a *tight-binding* description of the electronic orbitals,²⁶ and on the assumption of imperfect nesting between different Fermi surface sheets, the model of Ref. ²⁴ proposes a *f-wave* symmetry CDW gap with lobes along the saddle-point directions and six nodes at the points where the gap is zero (see Fig. 1). The proposed CDW gap is odd in the Brillouin zone due to the symmetry of the electron-phonon coupling,²⁴ and due to the absence of the inversion symmetry in the CDW phase, changing sign in each node. The superconductivity emerges from Cooper pairing between the Dirac fermions mediated by acoustic phonons via a piezoelectric coupling. We propose that the Fermi surface is fully gaped by the superposition of the CDW and the *s-wave* superconducting order parameters. This model is able to correctly explain some of the anomalous properties of the TMD such as the marginal quasiparticle lifetime in TaSe₂, the dependence of the normal-SC phase transition with the lattice parameters and the metallic behavior of the resistivity in the CDW phase.²⁴

The geometry of the proposed CDW gap is similar to the Brillouin zone of graphite, where the nodes represent the points where the conduction and valence π bands cross each other.²⁷ In contrast to graphite, the lattice inversion symmetry is broken in the distorted phase and piezoelectricity can arise. As it is usually observed in insulators since metals screen the polarization fields, one may ask, “is it actually possible to find piezoelectricity in a superconductor?” To answer this question, we should first consider that in a nodal liquid the density of states (DOS) goes to zero in the nodes, and therefore the electrons cannot effectively screen electric fields. Hence, one can conciliate a metallic theory (with gapless quasiparticle excitations) with the piezoelectricity. The rigorous vanishing of the DOS in the Fermi surface, however, is not essential for the piezoelectricity to appear. It is sufficient to consider that the electrons of low-lying momentum (for example, in a small pocket around the nodes) are “slow” enough to couple with the acoustic phonons of the polarized lattice.

If the piezoelectricity and the metallic character are not mutually excluding, it remains a question of how the polarization vector affects the phase coherence of the condensate. The answer to this second question can be found in the collective modes. The electromagnetic gauge invariance of the SC state is provided by the longitudinal response of the collective excitations, which screen the electrons through a cloud of virtual plasmons.²⁸ Only the plasmons respond to the longitudinal fields, and give rise to screening. Since the piezoelectricity involves electric fields only, it does not affect the phase coherence of the electrons. In a previous work,²⁹ we have shown by means of a semiclassical calculation that that piezoelectricity is not only consistent with the stability of the condensate as it is possibly behind the quantum critical points (QCPs) observed experimentally in the TaSe₂ phase diagram, separating the $T=0$ commensurate phases from the stripe phase as a function of the applied pressure.

The organization of the paper is as follows. In Sec. II we introduce the minimal model Hamiltonian of the CDW and SC phase. In Sec. III we derive the SC gap equation. Section IV is devoted to the thermodynamics of the SC phase, while

in Sec. V we calculate the acoustic attenuation rate and the nuclear magnetic relaxation (NMR) response. In Sec. VI we calculate the optical and thermal conductivities, in Sec. VII we discuss the Meissner effect. Finally, in Sec. VIII we present our conclusions.

II. THE HAMILTONIAN

The nodal system is composed of two subsystems defined by the nodes of the CDW state which are connected by the triple-CDW wave vectors \mathbf{Q}_i ($i=1,2,3$). It is convenient to introduce the spinors

$$\Psi_{i,\sigma}(\mathbf{k}) = \begin{pmatrix} c_{\mathbf{k},\sigma} \\ c_{\mathbf{k}+\mathbf{Q}_i,\sigma} \end{pmatrix} = \begin{pmatrix} \psi_{+,i,\sigma}(\mathbf{k}) \\ \psi_{-,i,\sigma}(\mathbf{k}) \end{pmatrix},$$

where $+$, $-$ indicate the two nodal spaces, and $c_{\mathbf{k},\sigma}^\dagger$ ($c_{\mathbf{k},\sigma}$) are creation (annihilation) operators for electrons with momentum \mathbf{k} and spin $\sigma = \uparrow, \downarrow$. The electronic Hamiltonian in the normal CDW phase is made of two terms

$$H_{\text{CDW}} = H_e + H_{e-c}.$$

H_e is the Hamiltonian of the free electrons in the vicinity of the nodes,

$$\begin{aligned} H_e &= \sum_{\mathbf{k},\sigma,i} [\epsilon_{\mathbf{k}} c_{\sigma,\mathbf{k}}^\dagger c_{\sigma,\mathbf{k}} + \epsilon_{\mathbf{k}+\mathbf{Q}_i} c_{\sigma,\mathbf{k}+\mathbf{Q}_i}^\dagger c_{\sigma,\mathbf{k}+\mathbf{Q}_i}] \\ &= \frac{1}{2} \sum_{\mathbf{k},a,b,\sigma,i} \psi_{a,i,\sigma}^\dagger(\mathbf{k}) \\ &\quad \times [(\epsilon_{\mathbf{k}} + \epsilon_{\mathbf{k}+\mathbf{Q}_i}) \eta_0^{ab} + (\epsilon_{\mathbf{k}} - \epsilon_{\mathbf{k}+\mathbf{Q}_i}) \eta_3^{ab}] \psi_{b,i,\sigma}(\mathbf{k}), \end{aligned} \quad (1)$$

where η_ν ($\nu=0,1,2,3$) are Pauli matrices that act in the nodal indexes $a, b = \pm$, and $\epsilon_{\mathbf{k}}$ is the free electron dispersion. In our convention, η_0 is the identity and $\nu=1,2,3$ indexes the x, y, z directions, respectively. The second term in the Hamiltonian, H_{e-c} , is the CDW exchange Hamiltonian between electrons situated in two different nodes connected by \mathbf{Q}_i ,

$$\begin{aligned} H_{e-c} &= \sum_{i,\mathbf{k}} \Delta_{c\mathbf{k}} c_{\mathbf{k},\sigma}^\dagger c_{\mathbf{k}+\mathbf{Q}_i} + \text{H.c.} \\ &= \sum_{i,\mathbf{k},\sigma,a,b} \Delta_{c\mathbf{k}} \psi_{a,i,\sigma}^\dagger(\mathbf{k}) \eta_1^{ab} \psi_{b,i,\sigma}(\mathbf{k}), \end{aligned} \quad (2)$$

where $\Delta_{c\mathbf{k}}$ is the CDW gap, with odd parity in the nodal space due to the loss of the lattice inversion symmetry. This term arises from the scattering of the electronic wave function by the CDW periodic superstructure.

Applying the *nesting* condition $\epsilon_{\mathbf{k}} + \epsilon_{\mathbf{k}+\mathbf{Q}} = 0$ (see Fig. 2) in Eq. (1), and taking the long-wavelength, low-energy limit, the Hamiltonian in the CDW phase reads,

$$H_{\text{CDW}} = \sum_{\mathbf{k},\sigma,i} \Psi_{i,\sigma}^\dagger(\mathbf{k}) [v_F k_\perp \eta_3 + v_\Delta k_\parallel \eta_1] \Psi_{i,\sigma}(\mathbf{k}) \quad (3)$$

where k_\perp and k_\parallel are the momentum components in the normal and parallel directions to the Fermi surface, respectively, v_F is the Fermi surface velocity, and $v_\Delta = \partial \Delta_c / \partial k_\parallel$. The CDW elementary excitations around the nodes are therefore fermi-

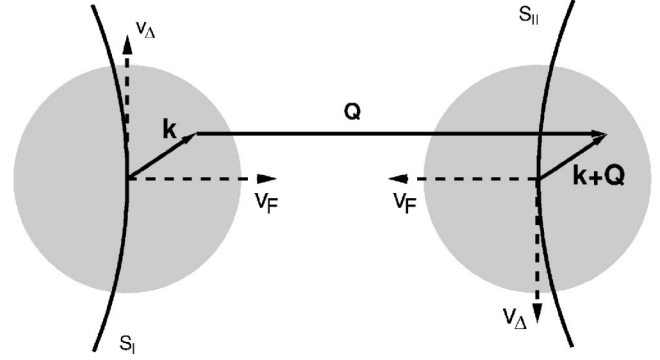


FIG. 2. Nesting condition in the two sheets S_I and S_{II} of the TMD Fermi surface. The momentum \mathbf{k} outside S_I is mapped by a CDW wave vector displacement into $\mathbf{k}+\mathbf{Q}$, inside S_{II} . As the free electron dispersion $\epsilon_{\mathbf{k}}$ is odd with respect to the Fermi surface sheets, we have $\epsilon_{\mathbf{k}} = -\epsilon_{\mathbf{k}+\mathbf{Q}}$.

ons which follow the 2D massless Dirac Hamiltonian, similarly to the two-band electronic description of graphite.²⁷

The broken lattice inversion symmetry due to the CDW gap allows piezoelectricity in the crystal. We propose that the electron-phonon coupling is piezoelectric, giving rise to a pairing of Dirac fermions in the singlet state through the triple-CDW superstructure. In contrast to the usual Cooper pairs, whose electrons are paired across the Fermi surface, these pairs are formed by electrons located in different nodes linked by a CDW wave vector \mathbf{Q}_i (see Fig. 1). The pairing approximation consists of assuming a condensate of pairs whose center-of-mass has momentum \mathbf{Q}_i and zero spin. This assumption clearly *violates* the time-reversal symmetry of the superconductor order parameter Δ_s . According to Anderson,³⁰ the strong insensibility of the BCS superconductors to impurities is due to the tendency of electrons to be in the state of highest possible degeneracy in the condensate, implying pairing each electron with its symmetric in spin and momentum. In such a case, the scattering channels promote transitions between two degenerated states, keeping the system coherent. The absence of time-reversal symmetry should destroy the condensate in the presence of a very small impurity concentration.³¹ In the case of TMD, however, the CDW scattering does not affect the degeneracy of the condensate as far as the Dirac fermions Ψ_i living in different nodal subspaces indexed by the three CDW directions $i=1,2,3$ remain decoupled. For this reason, we may drop the i index from now on.

After tracing the phonons, the piezoelectric pair interaction has the form²⁴

$$\begin{aligned} H_P &= -g \sum_{\mathbf{k},\mathbf{k}'} \sum_{a,b,c,d} \eta_2^{ab} \eta_2^{cd} \psi_{a,\uparrow}^\dagger(\mathbf{k}) \psi_{b,\downarrow}^\dagger(-\mathbf{k}) \\ &\quad \times \psi_{c,\uparrow}(\mathbf{k}') \psi_{d,\downarrow}(-\mathbf{k}'), \end{aligned}$$

where g is the piezoelectric coupling constant. The choice of the antisymmetric Pauli matrix η_2 incorporates the broken symmetry of the superconductor gap. In the mean-field approximation, the pairing Hamiltonian reads,

$$H_P = \sum_{\mathbf{k}} \sum_{a,b} [\Delta_s \psi_{a,\uparrow}^\dagger(\mathbf{k}) \eta_2^{ab} \psi_{b,\downarrow}^\dagger(-\mathbf{k}) + \text{H.c.}] + \frac{\Delta_s^2}{g}, \quad (4)$$

where

$$\Delta_s = -g \sum_{\mathbf{k}} \sum_{a,b} \langle \psi_{a,\uparrow}(\mathbf{k}) \eta_2^{ab} \psi_{b,\downarrow}(-\mathbf{k}) \rangle \quad (5)$$

is the complex superconductor order parameter.

So far, we have discussed the problem with particle-hole symmetry, that is, the chemical potential μ is exactly at the Dirac point ($\mu=0$). In order to include the situation where particle-hole symmetry is broken, we have added to Eq. (3) a chemical potential term

$$H_\mu = -\mu \sum_{\sigma,a} \psi_{a,\sigma}^\dagger(\mathbf{k}) \psi_{a,\sigma}(\mathbf{k}). \quad (6)$$

This term introduces an electronic ($\mu>0$) or hole ($\mu<0$) pocket around the Dirac point producing a finite density of states.

In order to diagonalize the problem, it is convenient to extend the spinorial notation to the Nambu space

$$\Psi(\mathbf{k}) = \begin{pmatrix} \psi_{+, \uparrow}(\mathbf{k}) \\ \psi_{+, \downarrow}^\dagger(-\mathbf{k}) \\ \psi_{-, \uparrow}(\mathbf{k}) \\ \psi_{-, \downarrow}^\dagger(-\mathbf{k}) \end{pmatrix}, \quad (7)$$

with \mathbf{k} defined with respect to the nodes. We introduce a new set of Pauli matrices τ_μ which operates in the space ($\uparrow k, \downarrow -k$). Denoting $\tau_\mu \eta_\nu$ as the tensor product between the Nambu and nodal spaces, it is not difficult to see that the full Hamiltonian is written as

$$H = \sum_{\mathbf{k}} \Psi^\dagger(\mathbf{k}) [v_F k_\perp \tau_0 \eta_3 + v_\Delta k_\parallel \tau_0 \eta_1 + \Delta_s \tau_1 \eta_2 - \mu \tau_3 \eta_0] \Psi(\mathbf{k}). \quad (8)$$

Notice that the gauge symmetry of the problem $\psi \rightarrow \psi e^{i\theta}$, and $\Delta_s e^{2i\theta} \rightarrow \Delta_s$ is broken at the mean-field level. With this notation, the SC order parameter is given by

$$\Delta_s = -g \sum_{\mathbf{k}} \langle \Psi^\dagger(\mathbf{k}) \tau_1 \eta_2 \Psi(\mathbf{k}) \rangle. \quad (9)$$

The diagonalization of the Hamiltonian above leads to four branches of excitations

$$\pm E_{\mathbf{k}, \pm \mu} \equiv \pm \sqrt{(v_F \bar{k} \pm \mu)^2 + \Delta_s^2}, \quad (10)$$

where $\bar{\mathbf{k}} = \bar{k}_\perp + (v_\Delta/v_F) \bar{k}_\parallel$ is the in-plane anisotropic momentum, with $\bar{k} \equiv |\bar{\mathbf{k}}|$. In the normal phase, we identify two branches of excitations (we assume $\mu > 0$):

$$\pm E_{\mathbf{k}, \pm \mu} \xrightarrow{\Delta_s \rightarrow 0} \begin{cases} \pm v_F \bar{k} + \mu & (\text{holelike branch}), \\ \pm v_F \bar{k} - \mu & (\text{particlelike branch}), \end{cases}$$

which are related to holelike and particlelike pockets around the CDW nodes (for $\mu < 0$, the nomenclature is exchanged). The two branches are physically equivalent to each other,

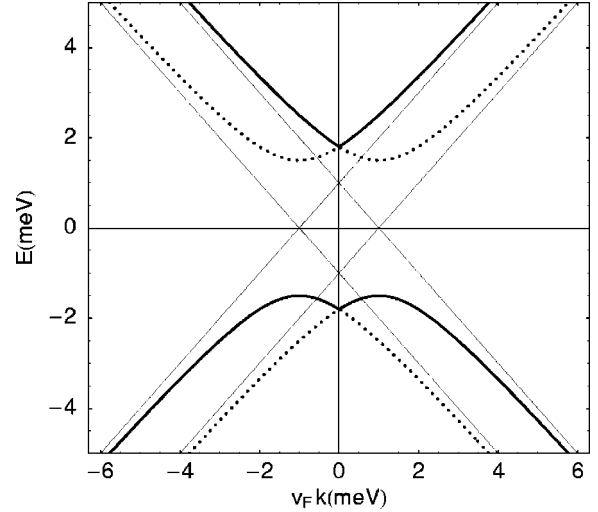


FIG. 3. Dirac fermions dispersion in the pocket with the opening of the SC gap for $|\mu| = \frac{3}{2} \Delta_s = 1$ meV. Each band has two pocket branches indicated by the dotted and thick solid lines. The thin solid lines with the vertex above (below) the Fermi energy $E=0$ represent the holelike (particlelike) branches of the Dirac cone in the normal CDW phase.

except for a constant equal to $-\sum_{\mathbf{k}} 2\mu$, integrated in the volume of the Dirac cone. The optical gap of the bands in the SC phase is $2\sqrt{\mu^2 + \Delta_s^2}$, as one can see from Fig. 3.

III. GAP EQUATION

To calculate the gap self-consistently, we use the standard many-body Green's function method. Since the Hamiltonian (8) is in the quadratic form $H = \sum_{\mathbf{k}} \Psi^\dagger \tilde{\omega} \Psi$, its corresponding Green function in 4×4 space is

$$\vec{G}(\mathbf{k}, i\omega_n) = - \int_0^\beta d\tau e^{i\omega_n \tau} \langle T_\tau [\Psi \Psi^\dagger] \rangle = (i\omega_n - \vec{\omega}_{\mathbf{k}})^{-1},$$

where T_τ is the time-ordering operator in imaginary time, ω_n are the fermionic Matsubara frequencies, $\beta = 1/(k_B T)$ is the inverse of temperature, k_B is the Boltzmann constant, and

$$\vec{\omega}_{\mathbf{k}} \equiv v_F \tau_0 \vec{\eta} \cdot \bar{\mathbf{k}} + \Delta_s \tau_1 \eta_2 - \mu \tau_3 \eta_0 \quad (11)$$

is the dispersion tensor with $v_F \vec{\eta} \cdot \bar{\mathbf{k}} \equiv v_F k_\perp \eta_3 + v_\Delta k_\parallel \eta_1$. Exploring the anticommutative property of the Pauli matrices, the Green function which is systematically used in our calculation is

$$\vec{G}(\omega_n, \mathbf{k}) = - (i\omega_n + \vec{\omega}_{\mathbf{k}}) \frac{\omega_n^2 + E_{\mathbf{k}}^2 + 2\mu v_F \tau_3 \vec{\eta} \cdot \bar{\mathbf{k}}}{[\omega_n^2 + E_{\mathbf{k}, \mu}^2][\omega_n^2 + E_{\mathbf{k}, -\mu}^2]}, \quad (12)$$

where

$$E_{\mathbf{k}}^2 \equiv v_F^2 \bar{k}^2 + \mu^2 + \Delta_s^2 = E_{\mathbf{k}, \pm \mu}^2 - 2v_F (\pm \mu) \bar{k}.$$

Noting that $\langle \Psi_\alpha^\dagger(\mathbf{k}) \Psi_\beta(\mathbf{k}) \rangle$ is the retarded part of the Green function $G_{\beta\alpha}(\mathbf{k}, \tau \rightarrow 0_-)$, we see from Eq. (9) that the amplitude of the mean-field gap is written in the Nambu spinorial notation as

$$2\Delta_s = -\frac{g}{\beta} \sum_{\mathbf{k}} \sum_{\omega_n=-\infty}^{\infty} \text{Tr}[\tau_1 \eta_2 \vec{G}(\omega_n, \mathbf{k})].$$

Evaluating the trace yields

$$2\Delta_s = \frac{g v_F \Delta_s}{2\pi v_\Delta} \sum_{\sigma=\pm 1} \int_0^\Lambda d\bar{k} \frac{\bar{k}}{E_{\mathbf{k},\sigma\mu}} \tanh\left(\beta \frac{E_{\mathbf{k},\sigma\mu}}{2}\right), \quad (13)$$

where Λ is a momentum cutoff associated with the linearization of the dispersion close to the CDW nodes.

For $\mu=0$, the gap equation is rather simple and reads

$$\Delta_s(T, g, \mu=0) = \frac{2}{\beta} \cosh^{-1}(\cosh[\pi v_\Delta v_F \beta / g_c] e^{-\pi v_\Delta v_F \beta / g}), \quad (14)$$

where $g_c = 2\pi v_\Delta / \Lambda$ is the zero-temperature critical coupling constant. In fact,

$$\Delta_s(T=0, g, \mu=0) = 2\pi v_\Delta v_F g_c^{-1} \left(1 - \frac{g_c}{g}\right). \quad (15)$$

Notice that for $g < g_c$ we find $\Delta_s(T=0, g < g_c, \mu=0) = 0$. Hence, the $\mu=0$ gap equation has a quantum critical point (QCP), indicating that superconductivity occurs only above a minimal coupling g_c . This is a general property of the nodal liquid, due to the absence of the background Fermi sea. In a Fermi liquid (where the Fermi surface is large in comparison to all other energy scales), the Fermi sea is unstable to the formation of Cooper pairs between two electrons mediated by an attractive potential, even for infinitesimal coupling.³² In this case, the Pauli exclusion principle of the background electrons plays the role of the interaction, making the condensate stable even in the weak coupling limit.³³ The zero temperature gap (15) equals the energy cutoff $\alpha = v_F \Lambda$ in the $g \rightarrow \infty$ limit.

A. Zero-temperature analysis

To see how the pocket affects the QCP when $g = g_c$ we analyze the gap equation in the zero-temperature limit. At this point, we introduce a more suitable cutoff, given by the momenta s_\pm that define the surfaces of constant energy in the Dirac cone

$$\alpha^2 \equiv v_F^2 \Lambda^2 = (v_F s_\pm \pm \mu)^2 + \Delta_s^2 = \text{const}. \quad (16)$$

This new definition of the cutoff (basically replacing Λ by s_σ , with $\sigma = \pm$) is convenient because it simplifies the integration, allowing us to find simple analytical expressions for the gap. This kind of approximation is fairly reasonable, since the results of this model are not to be taken literally when μ and Δ_s are comparable to the energy cutoff of the cone α , in which case the contribution of the high-energy states cannot be neglected. On the other hand, we should be warned by the fact that this new momentum cutoff s_σ does *not* conserve the number of states of the normal phase. When calculating thermodynamic functions, the correct cutoff is Λ , which correctly maps the volume of the Dirac cone and avoids problems such as losing states in the SC phase, which would certainly have an effect in the condensation energy. For al-

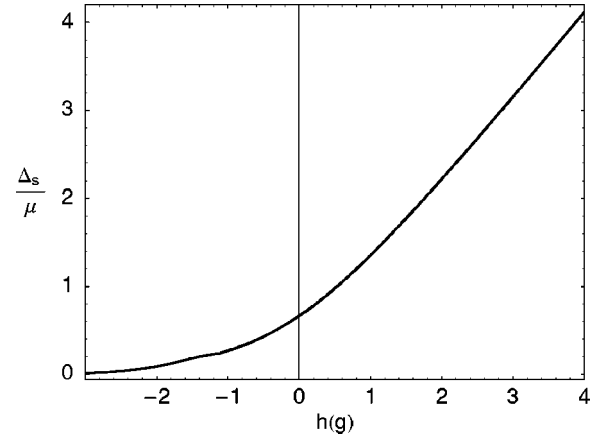


FIG. 4. Scaling of the zero temperature gap equation vs the coupling constant parameter $h(g) \propto (g_c^{-1} - g^{-1})/|\mu|$.

most all the applications, the results are not seriously affected by the details of the cutoff if the gap Δ_s is sufficiently small in comparison to α . The $T=0$ gap equation becomes

$$\begin{aligned} 2\Delta_s &= \frac{g v_F}{v_\Delta} \Delta_s \sum_{\sigma=\pm 1} \int_0^{s_\sigma} d\bar{k} \frac{\bar{k}}{2\pi E_{\mathbf{k},\sigma\mu}} \\ &= \frac{g}{2\pi v_F v_\Delta} \Delta_s \left[2\alpha - 2\sqrt{\Delta_s^2 + \mu^2} - \mu \ln\left(\frac{\sqrt{\Delta_s^2 + \mu^2} - \mu}{\sqrt{\Delta_s^2 + \mu^2} + \mu}\right) \right]. \end{aligned} \quad (17)$$

We rescale all the quantities by defining $x = \Delta_s / |\mu|$ and

$$h(g) = 2\pi v_F v_\Delta \frac{g_c^{-1} - g^{-1}}{|\mu|}.$$

The $T=0$ scale invariant equation is

$$F[x, h(g)] = \sqrt{1+x^2} + \frac{1}{2} \ln\left(\frac{\sqrt{1+x^2}-1}{\sqrt{1+x^2}+1}\right) - h(g) = 0. \quad (18)$$

We see in Fig. 4 that Eq. (18) has two distinct coupling regimes (i) the strong-coupling sector $g > g_c$, where the marginal physics develops, with $|\mu| \ll \Delta_s(0, g, \mu)$ for $g \gg g_c$ (strong-coupling limit) and (ii) the weak-coupling sector $g < g_c$, where the energy scale of the pocket is large in comparison to the gap [i.e., $|\mu| \gg \Delta_s(0, g, \mu)$] when $g/g_c \rightarrow 0$.

In the latter, the system flows in the direction of a Fermi liquid in the weak-coupling limit ($g \ll g_c$), while in the former the nodes are well defined for $g > g_c$, resulting in a nodal liquid description. We notice that the quasiparticle properties are strongly affected by the coupling constant g , which separates the marginal Fermi liquid (MFL) sector from the ‘‘Fermi-liquid’’ one, where the pocket plays the role of the Fermi surface, raising the density of states in the nodes.

For convenience, we denote the zero-temperature gap $\Delta_s(0, g, \mu)$ by $\Delta_{0\mu}$ from now on. In the strong-coupling limit ($|\mu|/\Delta_{0\mu} \ll 1$), we may write Eq. (17) as

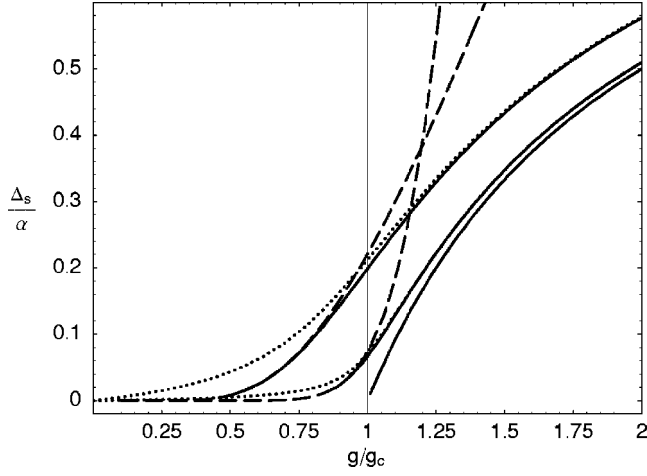


FIG. 5. Dependence of the zero temperature gap (normalized by the cutoff α) with the coupling constant g . Solid lines: numeric solution of the gap equation (18); dotted: strong coupling approximation ($|\mu| \ll \Delta_{0\mu}$); dashed: weak coupling one ($|\mu| \gg \Delta_{0\mu}$). We have set $|\mu|/\alpha = 0, 0.1$, and 0.3 from the bottom to the top. Notice that the QCP at $\mu=0$ is suppressed by the pocket formation ($|\mu| > 0$).

$$1 = \frac{g}{2\pi v_{\Delta} v_F} \left(\alpha - \Delta_s + \frac{\mu^2}{2\Delta_s} \right),$$

whose solution is

$$\Delta_{0\mu} \xrightarrow{g \gg g_c} \frac{\Delta_0}{2} (1 + \sqrt{1 + 2\mu^2/\Delta_0^2}), \quad (19)$$

where $\Delta_0 \equiv \Delta(T=0, g, \mu=0)$ is given by Eq. (15). In the opposite limit $\Delta_{0\mu}/|\mu| \ll 1$ in the weak-coupling sector, we see that Eq. (18) can be expanded in leading order in x , giving

$$\begin{aligned} F[x, h(g)] &\xrightarrow{x \rightarrow 0} 1 + \ln\left(\frac{x}{2}\right) - h(g) \\ &= 1 + \ln\left(\frac{\Delta_s}{2|\mu|}\right) - 2\pi v_F v_{\Delta} \frac{g_c^{-1} - g^{-1}}{|\mu|} = 0, \end{aligned}$$

yielding

$$\Delta_{0\mu} \xrightarrow{g \ll g_c} 2|\mu| e^{h(g, \mu)-1} = 2|\mu| e^{2\pi v_F v_{\Delta} (g_c^{-1} - g^{-1}) |\mu|^{-1} - 1}. \quad (20)$$

Although the strong-coupling approximation is rigorously valid for $g \gg g_c$ and the weak-coupling one for $g \ll g_c$, these two approximations are remarkably good in almost the entire coupling range of their respective sectors (as shown in Fig. 5) provided that μ/α is small. However, to find sensible results, one should consider that the valid coupling range of the theory is limited not too far above the critical coupling g_c , in order to keep the ratio $\Delta_{0\mu}/\alpha$ small (see Fig. 5).

B. Finite temperature

Let us return to Eq. (13). After some algebraic manipulation (see the details in Appendix A), the gap equation in the strong-coupling regime assumes the form

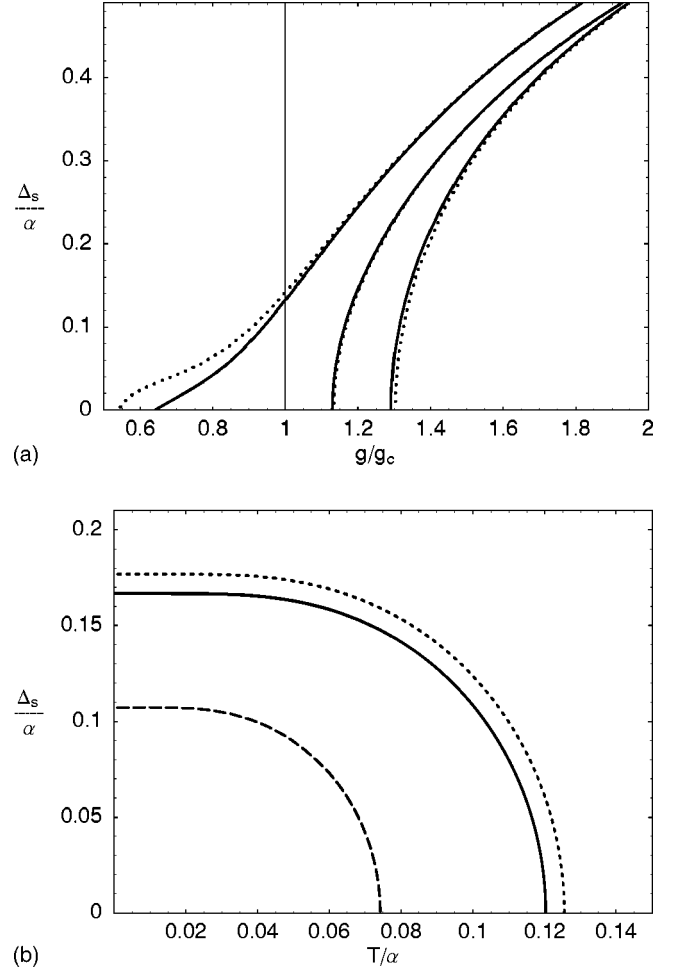


FIG. 6. Top: SC gap $\Delta_s(T, g, \mu)$ vs the coupling constant g/g_c . Solid lines: numeric solution of the gap equation (13); dotted lines: strong coupling solution (analytic). From left to right: $k_B T/\alpha = 0.005, 0.1, 0.2$ and $|\mu|/\alpha = 0.2, 0.2, 0.1$, respectively. Bottom: SC gap vs temperature. The scales are normalized by the energy cutoff α of the Dirac cone. Dotted line: ($|\mu|/\alpha = 0.06, g/g_c = 1.2$); solid: ($\mu/\alpha = 0, g/g_c = 1.2$); dashed: ($|\mu|/\alpha = 0.06, g/g_c = 1.1$).

$$\begin{aligned} &\cosh(\beta\Delta_s/2) e^{-\mu^2\beta \tanh(\beta\Delta_s/2)/(4\Delta_s)} \\ &= \cosh(\pi v_{\Delta} v_F \beta/g_c) e^{-\pi v_{\Delta} v_F \beta/g}. \end{aligned} \quad (21)$$

The quantity $\tanh[\beta\Delta_s/2]/\Delta_s$ changes very little with β in the whole temperature interval. In a first approximation, we can obtain the analytical expression of the low-temperature gap by replacing the gap inside the exponential above by its zero-temperature value $\Delta_{0\mu}$. This substitution leads to:

$$\begin{aligned} \Delta_s(T, g, \mu) &\sim \frac{2}{\beta} \cosh^{-1}[\cosh(\pi v_{\Delta} v_F \beta/g_c)] \\ &\times e^{-\pi v_{\Delta} v_F \beta/g} e^{\mu^2\beta \tanh(\beta\Delta_{0\mu}/2)/(4\Delta_{0\mu})}, \end{aligned}$$

valid at strong coupling for small μ/α . Close to the phase transition, Eq. (13) yields

$$\Delta_s(T) \xrightarrow{T \rightarrow T_c} \begin{cases} 2\sqrt{\frac{\Delta_0}{\beta_c} + \frac{\mu^2}{2}} t^{1/2}, & |\mu|/\Delta_{0\mu} \ll 1, \\ \frac{1}{\beta_c} \left[\frac{7\zeta(3)}{8\pi^2} + \frac{1}{2\beta_c^2 \mu^2} \right]^{-1/2} t^{1/2}, & |\mu|/\Delta_{0\mu} \gg 1, \end{cases} \quad (22)$$

where $t \equiv (T_c - T)/T_c$ is the reduced temperature and ζ is the Zeta function. The critical temperature is also calculated from the gap Eq. (13) in the $\Delta_s \rightarrow 0$ limit, giving

$$T_c = \begin{cases} \frac{1}{2k_B \ln 4} [\Delta_0 + \sqrt{\Delta_0^2 + \mu^2 \ln 4}], & |\mu|/\Delta_{0\mu} \ll 1, \\ \frac{|\mu| \gamma}{k_B \pi} e^{\alpha(1-g_c/g)|\mu|^{-1}}, & |\mu|/\Delta_{0\mu} \gg 1, \end{cases} \quad (23)$$

where $\ln \gamma \sim 0.577$ is the Euler constant. In the particle-hole symmetric case ($\mu=0$), we have $T_c = \Delta_0/(k_B \ln 4)$ and $\Delta_s(T \rightarrow T_c, g, 0) = 2\Delta_0 t^{1/2}/\ln 2$ (see Appendix A for details).

We see that the existence of a pocket suppresses the QCP ($T=0$) separating the normal and SC phases (see Fig. 5). This effect is due to the establishment of the background Fermi sea, which stabilizes the Cooper pairs for an arbitrarily small coupling. The thermal effect on the gap recovers the parametric phase transition with the coupling constant g , as displayed in Fig. 6 (top) by noting the presence of a minimal coupling [say, $g_0(T, \mu)$, with $g_0(0, 0) = g_c$], below which $\Delta_s(g < g_0, \mu) = 0$. The explanation can be found in the strong dependence of the critical temperature T_c with g , as shown in Fig. 6 (bottom). At a given nonzero temperature T , a minimal coupling is required to satisfy $T_c(g > g_0) > T$.

IV. THERMODYNAMICS

In this section, we calculate the thermodynamic functions starting from the partition function Z of the nodal fermions. The partition function is defined as usual from the original Hamiltonian (8), written in a diagonal basis of eigenstates indexed by \mathbf{k} , $\gamma = \pm 1$ (for the two particle-hole branches), $\sigma = \pm 1$, and with eigenvalues $E_{\mathbf{k}}^a = \pm E_{\mathbf{k}, \sigma \mu}$,

$$\begin{aligned} Z &= e^{-\beta\Omega} = \text{tr} e^{-\beta H} \\ &= e^{-\beta g^{-1} \Delta_s^2} \prod_{\mathbf{k}, a} \sum_{n_{\mathbf{k}}^a=0}^1 \langle n_{\mathbf{k}}^a | e^{-\beta E_{\mathbf{k}}^a n_{\mathbf{k}}^a} | n_{\mathbf{k}}^a \rangle \\ &= e^{-\beta g^{-1} \Delta_s^2} \prod_{\mathbf{k}, \gamma, \sigma} (1 + e^{-\beta \gamma E_{\mathbf{k}, \sigma \mu}}), \end{aligned}$$

where Ω is the thermodynamic potential. The Hamiltonian includes the term Δ_s^2/g , in order to give the correct condensation energy. The thermodynamic potential $\Omega = \Omega_0 + \Delta_s^2/g$ is given by

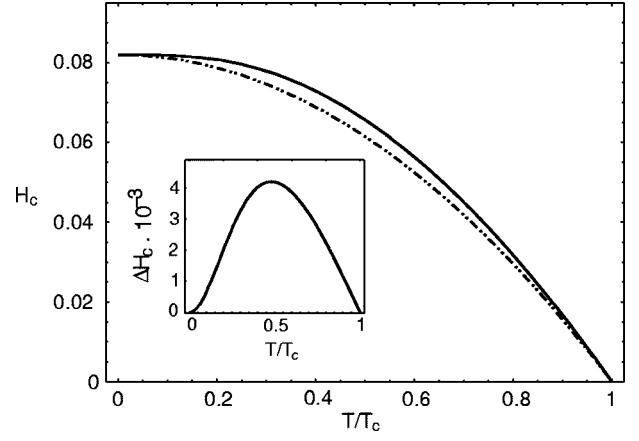


FIG. 7. Solid line: critical field H_c dependence with temperature, in units of $\sqrt{(\alpha^2/g_c)}$ for $\mu=0$ and $g/g_c=1.1$; dotted: empirical law $H_c(0)[1 - T^2/T_c^2]$. The difference between the two curves is shown in the inset.

$$\begin{aligned} \Omega_0(T) &= -\frac{1}{\beta} \sum_{\mathbf{k}, \sigma} \ln[2 + 2 \cosh(\beta E_{\mathbf{k}, \sigma \mu})] \\ &= -\frac{v_F}{\pi \beta v_{\Delta}} \sum_{\sigma} \int_0^{\Lambda} d\bar{k} \bar{k} \ln[2 + 2 \cosh(\beta E_{\mathbf{k}, \sigma \mu})]. \end{aligned} \quad (24)$$

If Ω_n is the thermodynamic potential in the normal phase, the energy of condensation $\Omega_n(0) - \Omega_0(0) = H_c^2(0)/(8\pi)$ is given in terms of the zero-temperature critical field H_c , shown in Fig. 7. The internal energy $E = E_0 + \Delta_s^2/g$ is given by

$$\begin{aligned} E_0(T) &= \sum_{\mathbf{k}, \gamma, \sigma} \gamma E_{\mathbf{k}, \sigma \mu} n_{\mathbf{k}}^{\gamma} \\ &= -\frac{v_F}{2\pi v_{\Delta}} \sum_{\sigma} \int_0^{\Lambda} d\bar{k} \bar{k} E_{\mathbf{k}, \sigma \mu} \tanh\left(\frac{\beta E_{\mathbf{k}, \sigma \mu}}{2}\right). \end{aligned} \quad (25)$$

where $n_{\mathbf{k}}^{\gamma} = (e^{\gamma \beta E_{\mathbf{k}, \sigma \mu}} + 1)^{-1}$ is the Fermi-Dirac distribution indexed in σ , $\gamma = \pm 1$.

According to the usual thermodynamic relations, the specific heat is defined by

$$C_V = T \frac{dS}{dT} = -\beta \frac{dS}{d\beta}, \quad (26)$$

where $S = (E - \Omega)/T = -(\partial \Omega / \partial T)_V$ is the electronic entropy due to the Dirac fermions. At low temperature, the gap is practically independent of temperature. It is easy to check that the specific-heat dependence with temperature in this limit for $\mu=0$ is given by:

$$\begin{aligned} C_V &\xrightarrow{T \ll T_c} \frac{1}{2\pi v_F v_{\Delta}} \int_{\Delta_s}^{E_{\Lambda}} dE E^3 \text{sech}^2\left(\frac{\beta E}{2}\right) \\ &\xrightarrow{\Lambda \rightarrow \infty} \frac{6k_B}{\pi v_F v_{\Delta}} \Delta_s^2 e^{-\beta \Delta_s}, \end{aligned}$$

leading to the expected exponential behavior with the gap. A more interesting result is related to the jump of the specific

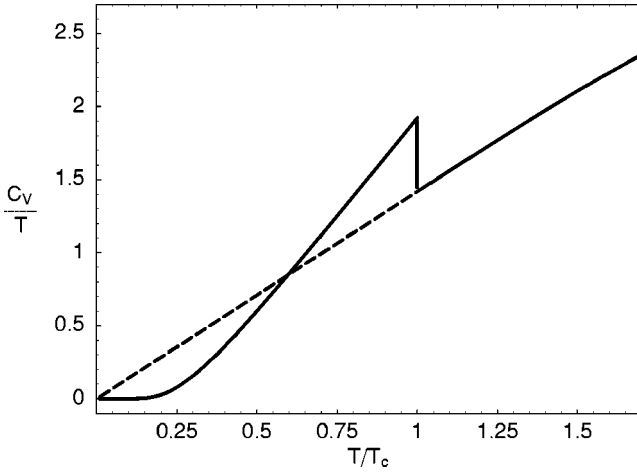


FIG. 8. Specific heat $C_V \times 1/T$ vs temperature for $\mu=0$, in units of k_B^2/g_c . The jump occurs at $k_B T_c = \Delta_0/\ln 4$. Dashed line: normal behavior in the absence of the SC gap.

heat in the normal-SC phase transition. The calculation is given in Appendix B for the weak- and strong-coupling regimes. It results in two well defined limits: the marginal one ($|\mu|\beta_c \ll 1$),

$$\left. \frac{\Delta C_V}{C_{n,v}} \right|_{T_c} = \frac{2 \ln 4}{9\zeta(3)} \left(\ln 4 + \frac{\beta_c^2 \mu^2}{2} \right) \geq 0.35,$$

where the equality holds for $\mu=0$, and the Fermi-liquid limit

$$\left. \frac{\Delta C_V}{C_{n,v}} \right|_{T_c} = \frac{3}{2\pi^2} \frac{1}{7\zeta(3) + \frac{1}{8\pi^2 + 2\beta_c^2 \mu^2}} \leq 1.43, \quad (27)$$

which recovers the BCS result for $\beta_c |\mu| \gg 1$. The jump observed in the NbSe₂ crystal^{34–36} ($\Delta C/C_n \sim 2$) is a good indication in favor of a conventional Fermi liquid and BCS behavior. In TaSe₂, however, where the transport is marginal and the quasiparticles are not well defined in the Landau sense³⁷ ($\tau\omega < 1$, where τ^{-1} is the scattering rate), the picture can be very different. In the nodal liquid case, the specific-heat jump is strongly attenuated due to the vanishing density of states (DOS) in the Fermi surface, resulting in the universal constant $\Delta C_V/C_n = 0.35$. The plot of the specific heat displayed in Fig. 8 shows that the temperature dependence of the normal CDW phase is quadratic. As the DOS is raised by a pocket around the nodes, the jump grows in the direction of the BCS value of 1.43, which corresponds to the weak-coupling limit. However, we notice that the nodes cease to be well defined in the presence of large pockets. In this case, the pairing ansatz adopted in Sec. II and the role of piezoelectricity in the electron-phonon coupling are questionable.

V. COHERENCE FACTOR EFFECTS

In this section we calculate two basic properties of the superconductor: the acoustic attenuation and the nuclear-spin-relaxation rate in the absence of impurities.

A. Acoustic attenuation

The ultrasound attenuation results from the resonant absorption of the longitudinal phonons in the solid.³⁸ The absorption rate is proportional to the imaginary part of the charge susceptibility³⁹

$$\alpha_s(\mathbf{q}) = -\lambda_1^2 \lim_{\omega \rightarrow 0} \left[\frac{1}{\omega} \text{Im} \chi^c(\mathbf{q}, \omega) \right] \quad (28)$$

in the $q \rightarrow 0$ limit, since the phonon wavelength is much larger than the typical electronic wavelength. This property is connected to the superconductor *coherence factors*, which basically define the probability amplitude of quasiparticle transitions between two states represented by the pairs space ($\mathbf{k}\uparrow, -\mathbf{k}\downarrow$).^{33,38} These factors conserve the time reversal symmetries of the interaction involved in the transition. They are usually divided into type I, for interactions which preserve the time-reversal symmetry (as in the electron-phonon coupling) and type II when this symmetry is broken, as in the spin-exchange interaction. The charge susceptibility is defined in terms of the time-ordered charge-density correlation function. All the correlation functions used in this article are defined in Appendix C. Using the spinor defined in (7) the charge-density operator is given by

$$\begin{aligned} \rho(\mathbf{q}) &= \sum_{\mathbf{k}, \sigma, a} \psi_{a\sigma}^\dagger(\mathbf{k} - \mathbf{q}/2) \psi_{a\sigma}(\mathbf{k} + \mathbf{q}/2) \\ &= \sum_{\mathbf{k}} \Psi^\dagger(\mathbf{k} - \mathbf{q}/2) \tau_3 \eta_0 \Psi(\mathbf{k} + \mathbf{q}/2). \end{aligned} \quad (29)$$

We define $\vec{G}_+ \equiv \vec{G}(\mathbf{k} + \mathbf{q}/2, i\omega_n + i\omega)$ and $\vec{G}_- \equiv \vec{G}(\mathbf{k} - \mathbf{q}/2, i\omega_n)$, so that the electronic charge susceptibility reads

$$\chi^c(\mathbf{q}, i\omega) = \frac{1}{\beta} \text{Tr} \sum_{\mathbf{k}, \omega_n} \vec{G}_+ \tau_3 \eta_0 \vec{G}_- \tau_3 \eta_0. \quad (30)$$

It is convenient to define the gapless Dirac fermions dispersion by $\epsilon_{\mathbf{k}} = v_F \bar{k}$, and the quantity $\epsilon^0 = \sqrt{v_F^2(\bar{k}^2 + \bar{q}^2)/4}$. After evaluating the trace and the sum over the fermionic Matsubara frequencies, the imaginary part of the susceptibility reads:

$$\begin{aligned} \text{Im} \chi^c(\mathbf{q}, \omega \rightarrow 0) &= \frac{\omega}{\epsilon_{q/2}} \frac{v_F}{\pi v_\Delta} \int_0^\Lambda dkk \sum_{\sigma=\pm 1} \frac{\partial n(E_{\sigma\mu}^0)}{\partial E_{\sigma\mu}^0} \\ &\times \frac{\epsilon^0 + \sigma\mu}{\epsilon^0 E_{\sigma\mu}^0} \sqrt{(\epsilon^0)^2 - \epsilon_{q/2}^2}, \end{aligned} \quad (31)$$

where $E_{\sigma\mu}^0 = \sqrt{(\epsilon^0 + \sigma\mu)^2 + \Delta_s^2}$, and n is the Fermi-Dirac distribution. Replacing Eq. (31) into Eq. (28), we obtain the ultrasound attenuation rate

$$\alpha_s \xrightarrow{q \rightarrow 0} -\frac{1}{\epsilon_{q/2}} \frac{\lambda_1^2}{\pi v_\Delta v_F} \sum_{\sigma=\pm 1} \int_0^\alpha \frac{d\epsilon\epsilon}{E_{\sigma\mu}} (\epsilon + \sigma\mu) \frac{\partial n(E_{\sigma\mu})}{\partial E_{\sigma\mu}}.$$

The temperature dependence is displayed in Fig. 9 and shows a power-law behavior near the phase transition. This result is compared with the BCS curve $\alpha_s/\alpha_n = 2/(e^{\beta\Delta_s} + 1)$.³³

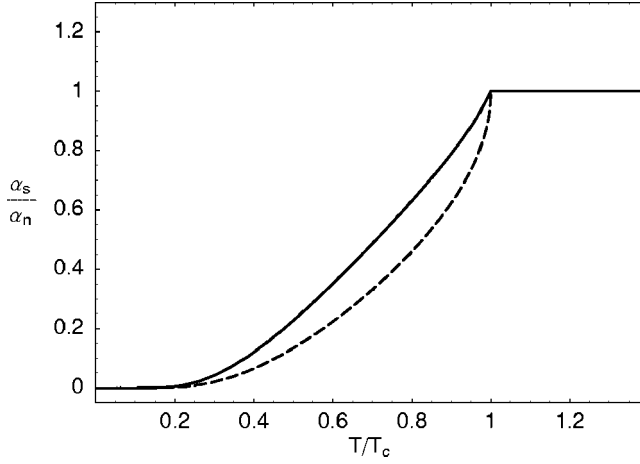


FIG. 9. Temperature dependence of the acoustic attenuation rate normalized by the normal phase rate. Solid: this model ($\mu=0$ and $g/g_c=1.1$); dashed: BCS model.

B. NMR relaxation

The NMR relaxation has its origin on the hyperfine interaction between the nuclear spins and the electrons. The relaxation rate measures the nuclear-spin time variation along an arbitrary direction of the spin space, say $\hat{\mathbf{b}}$. The condensate exhibits no paramagnetism in the singlet channel, where the total spin of the pairs is zero. Since the Zeeman and hyperfine energies are usually small in comparison to the gap, the only processes that contribute to the spin relaxation are thermally excited quasiparticles. The inverse of the spin relaxation is proportional to the local magnetic susceptibility projected along $\hat{\mathbf{b}}$,

$$T_1^{-1}(\hat{\mathbf{b}}) = -\lambda_2^2 \sum_{\mathbf{q}} \lim_{\omega \rightarrow 0} \left[\frac{1}{\omega} \text{Im} \chi_{\mathbf{b}}^s(\mathbf{q}, \omega) \right], \quad (32)$$

where $\chi_{\mathbf{b}}^s(\omega)$ is given in terms of the normal directions of the spin space by $\chi_{\mathbf{b}}^s(\omega) = \sum_{ij} (\delta^{ij} - b^i b^j) \chi_{ij}^s(\omega)$, with $i, j=1, 2, 3$ representing the x, y, z directions, respectively (see Appendix C).

Before defining the spin-density operator, we must introduce the spin degrees of freedom in the spinor representation, Eq. (7). This is naturally done in the Balian-Werthamer (BW) space⁴⁰

$$\Psi_a(\mathbf{k}) = \begin{pmatrix} \zeta_a(\mathbf{k}) \\ -i\sigma_2 \zeta_a^\dagger(-\mathbf{k}) \end{pmatrix} = \begin{pmatrix} \psi_{a\uparrow}(\mathbf{k}) \\ \psi_{a\downarrow}(\mathbf{k}) \\ -\psi_{a\downarrow}^\dagger(-\mathbf{k}) \\ \psi_{a\uparrow}^\dagger(-\mathbf{k}) \end{pmatrix} \quad (33)$$

which contains an additional spin subspace

$$\zeta(\mathbf{k}) = \begin{pmatrix} \psi_{\uparrow}(\mathbf{k}) \\ \psi_{\downarrow}(\mathbf{k}) \end{pmatrix}$$

inside the regular Nambu space, ($\uparrow\mathbf{k}, \downarrow-\mathbf{k}$). We have defined a new set of Pauli matrices $\sigma_{\mu} = (\sigma_0, \vec{\sigma})$ which operates in this new space. The general spin-density operator is

$$\begin{aligned} S_i(\mathbf{q}) &= \frac{1}{2} \sum_{\mathbf{k}\sigma\sigma'a} \psi_{a,\sigma}^\dagger(\mathbf{k}-\mathbf{q}/2) \sigma_i^{\sigma\sigma'} \psi_{a,\sigma'}(\mathbf{k}+\mathbf{q}/2) \\ &= \frac{1}{2} \sum_{\mathbf{k} \in \frac{1}{2}\text{BZ}} \Psi^\dagger(\mathbf{k}-\mathbf{q}/2) \sigma_i \tau_0 \eta_0 \Psi(\mathbf{k}+\mathbf{q}/2), \end{aligned} \quad (34)$$

where $i=1, 2, 3$ are the spin directions, \mathbf{k} is summed in the half Brillouin zone, and $\sigma, \sigma' = \uparrow \downarrow$ are the spin indexes. It is not difficult to check that the Hamiltonian (8) written in the BW space is given by (see Appendix D)

$$H = \sum_{\mathbf{k} \in \frac{1}{2}\text{BZ}} \Psi^\dagger(\mathbf{k}) [v_F \sigma_0 \tau_0 \vec{\eta} \cdot \bar{\mathbf{k}} - \Delta_s \sigma_3 \tau_1 \eta_2 - \mu \sigma_0 \tau_3 \eta_0] \Psi(\mathbf{k}). \quad (35)$$

The matrix inside the parenthesis defines the new dispersion tensor $\vec{\omega}_{\mathbf{k}}$ of the Green function (12), $\vec{G} = (i\omega_n - \vec{\omega})^{-1}$. Notice that the BW Green function is very similar to the previous one, except for the size of the Hamiltonian space, which is now 8×8 .

The pairing term brings something new because of the broken time-reversal symmetry of the SC phase, expressed by the antisymmetric property of the Pauli matrix η_2 under the transposition $\eta_\alpha^{ab} \rightarrow \eta_\alpha^{ba}$. We will soon explore the physical consequences of this broken symmetry. From Eq. (C2) the spin susceptibility tensor is given by

$$\chi_{ij}^s(\mathbf{q}, i\omega) = \frac{1}{4\beta} \text{Tr} \sum_{\mathbf{k} \in \frac{1}{2}\text{BZ}} \sum_{\omega_n} \vec{G}_+ \sigma_i \tau_0 \eta_0 \vec{G}_- \sigma_j \tau_0 \eta_0. \quad (36)$$

Notice that the product $\sigma_i \tau_0 \eta_0 \vec{G}_+ \sigma_i \tau_0 \eta_0 = \vec{G}$ for $i=3$. For $i=1, 2$, the anticommutative matrices η_i lead to a sign change in the gap term of $\vec{\omega}$ inside the Green function, meaning $\Delta_s \rightarrow -\Delta_s$. Thus, the $i=1, 2$ (i.e., x, y) directions have the same coherence factors of the charge susceptibility

$$\chi_{xx}^s(\mathbf{q}, \omega) = \chi_{yy}^s(\mathbf{q}, \omega) = \frac{1}{4} \chi^c(\mathbf{q}, \omega). \quad (37)$$

This property is better illustrated in the $\mu=0$ case, where

$$\chi_{xx}^s = \frac{1}{\beta} \sum_{\mathbf{k}, \omega_n} \frac{(\vec{\epsilon}_- \cdot \vec{\epsilon}_+ - \Delta_s^2) - \omega_n(\omega_n + \omega)}{[\omega_n^2 + E_-^2][(\omega_n + \omega)^2 + E_+^2]} = \chi_{yy}^s,$$

$$\chi_{zz}^s = \frac{1}{\beta} \sum_{\mathbf{k}, \omega_n} \frac{(\vec{\epsilon}_- \cdot \vec{\epsilon}_+ + \Delta_s^2) - \omega_n(\omega_n + \omega)}{[\omega_n^2 + E_-^2][(\omega_n + \omega)^2 + E_+^2]},$$

with $\vec{\epsilon}_{\pm} \equiv v_F \bar{\mathbf{k}}$ and the indexes \pm representing the momentum $\pm \rightarrow \mathbf{k} \pm \mathbf{q}/2$. Notice the sign difference in front of Δ_s^2 between the zz and the other two components. This gives rise to an axial anisotropy in the z direction of the spin space. This anisotropy is a consequence of the broken time-reversal symmetry induced by the finite momentum of the pairs \mathbf{Q}_i , which defines the CDW wave vectors. This broken symmetry is reflected in the appearance of the spin structure oriented in the z direction of the spin space (indicated by the σ_3 matrix) in the pairing term of the BW Hamiltonian (35). Therefore, we conclude that the z direction of the spin space corre-

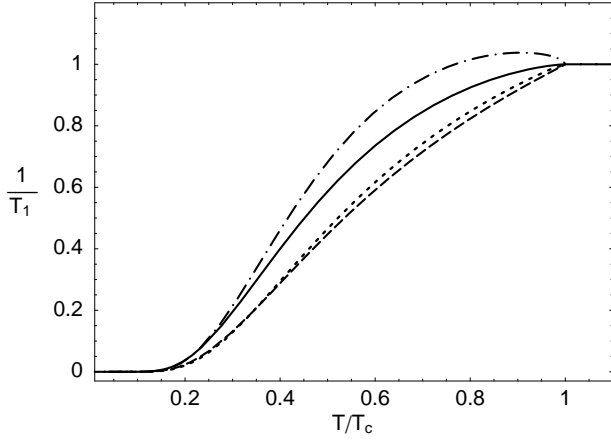


FIG. 10. Temperature dependence of the NMR relaxation rate normalized by the normal phase relaxation for $g/g_c=1.1$. Dashed ($\mu=0$) and dotted ($|\mu|/\alpha=0.05$) lines: NMR response along the in-plane directions [$\varphi=\pi/2$ case of Eq. (40)]; solid ($\mu=0$) and dot-dashed ($|\mu|/\alpha=0.05$) lines: NMR response along the normal c -axis ($\varphi=0$). The pocket produces a small Hebel-Slichter peak, indicated by the dot-dashed line.

sponds to the CDW direction \mathbf{Q}_i in the k space, since it is the only rotational symmetry broken in the crystal. The calculation of the imaginary part of the χ_{zz}^s susceptibility reads

$$\begin{aligned} & \text{Im } \chi_{zz}^s(\mathbf{q}, \omega \rightarrow 0) \\ &= \frac{\omega v_F}{4\pi v_\Delta} \int_0^\Lambda dkk \left\{ \frac{\partial n(\tilde{E})}{\partial \tilde{E}} \frac{2\Delta_s^2 \epsilon_{q/2}^2 - \mu^2}{\tilde{\epsilon}_k \tilde{E} \tilde{\epsilon}_k^2 - \mu^2} \right. \\ & \quad \times \text{Re} \left[\frac{\theta(\tilde{\epsilon}_k - |\mu|) \tilde{\epsilon}_k + \theta(|\mu| - \tilde{\epsilon}_k) |\mu|}{\sqrt{(\epsilon_{q/2}^2 - \mu^2)(\tilde{\epsilon}_k^2 - \epsilon_{q/2}^2)}} \right] \\ & \quad \left. + \sum_{\sigma=\pm 1} \frac{\partial n(E_{\sigma\mu}^0)}{\partial E_{\sigma\mu}^0} \frac{E_{\sigma\mu}^0}{(\epsilon^0 + \sigma\mu)} \frac{\sqrt{(\epsilon^0)^2 - \epsilon_{q/2}^2}}{\epsilon_{q/2} \epsilon^0} \right\}, \quad (38) \end{aligned}$$

where

$$\tilde{\epsilon}_k = \text{Re} \sqrt{\epsilon_k^2 + \epsilon_{q/2}^2 - \mu^2},$$

$\tilde{E}_k = \sqrt{\tilde{\epsilon}_k^2 + \Delta_s^2}$, and $\epsilon^0, E_{\sigma\mu}^0$ follow the definitions of the previous subsection. The $\chi_{xx,yy}^s$ can be obtained from the substitution of Eq. (31) into Eq. (37). Noting that $\chi_{xy}^s = \chi_{xz}^s = \chi_{yz}^s = 0$, the contribution of each CDW wavevector \mathbf{Q}_j ($j=1,2,3$) to the NMR relaxation rate along a given direction $\hat{\mathbf{b}}$ gives

$$\frac{1}{T_1}(\hat{\mathbf{b}}) = \lambda_2^2 \int_0^\Lambda \frac{d\bar{q}}{2\pi} \bar{q} \lim_{\omega \rightarrow 0} \left[\frac{1}{\omega} \sum_i (b_i^2 - 1) \text{Im} \chi_{ii}^s \right] \quad (39)$$

In Fig. 10 we distinguish the two principal directions, for in-plane $\hat{\mathbf{b}}$ vectors and out-of-plane ones directed along the normal c -axis. A small Hebel-Slichter peak is formed for finite μ , but no peak is observed for $\mu=0$.

The zz component of the susceptibility carries coherence factors with the symmetry of the spin interactions (i.e., they are odd by interchanging $\mathbf{k} \rightarrow -\mathbf{k}$), while the xx and yy components are analogous to the charge susceptibility [see Eq.

(37)]. This is easily understood by a qualitative argument with the aid of Eq. (39). Consider the CDW direction \mathbf{Q}_1 for the moment. The \mathbf{Q}_1 direction (or, equivalently, the $\mathbf{b}=\hat{z}$ direction for the spin, according to our previous discussion) affects the electronic spin correlations in the normal directions to \mathbf{Q}_1 , meaning the xy plane. The NMR direction $\mathbf{b}=\hat{z}$ is affected by the susceptibility components χ_{xx} and χ_{yy} but not by the χ_{zz} one [see Eq. (39)]. The CDW introduces an additional time-reversal broken symmetry to the spin correlations in the \mathbf{Q}_1 (xy) plane, explaining why the related coherence factors have the same symmetry of the charge interactions. On the other hand, the planes which are normal to the \mathbf{Q}_1 plane are affected by the χ_{zz} component, which conserves the odd symmetry of the spin interactions. In summary, the NMR relaxation in the $\hat{\mathbf{b}}=\mathbf{Q}_1$ direction (in k space) is therefore associated to a *chargelike* symmetry, as in the phonon attenuation response, while the NMR directions which are normal to \mathbf{Q}_1 have a mixed symmetry and exhibit a more intense response. The same analysis applies to the $\mathbf{Q}_{2,3}$ vectors separately. The NMR pattern in k space for the SC planes results from the superposition of the contributions due to each vector \mathbf{Q}_i ($i=1,2,3$) of the triple CDW. As each vector \mathbf{Q}_i is rotated with respect to the other two by $2\pi/3$ and $4\pi/3$ (see Fig. 1), if we define the contribution of each CDW wavevector to the NMR response along an arbitrary direction $\hat{\mathbf{b}}$, as $T_{1,i}^{-1}(\hat{\mathbf{b}}) = T_1^{-1}(\hat{\mathbf{b}} + \theta_i)$, with $\theta_i = 0, 2\pi/3, 4\pi/3$ respectively for $i=1,2,3$, it is not difficult to vary from Eq. (39) that

$$\begin{aligned} \sum_i \frac{1}{T_{1,i}}(\hat{\mathbf{b}}) &= -3\lambda_2^2 \int_0^\Lambda \frac{d\bar{q}}{2\pi} \bar{q} \lim_{\omega \rightarrow 0} \frac{1}{\omega} \\ & \quad \times \left[\text{Im} (\chi_{xx}^s + \chi_{yy}^s) + \frac{1}{2} \sin^2 \varphi \text{Im} (\chi_{xx}^s - \chi_{zz}^s) \right], \quad (40) \end{aligned}$$

where φ is the angle that $\hat{\mathbf{b}}$ makes with the normal direction to the SC planes. We notice that despite the broken rotational symmetry of the triple-CDW state, the total NMR response is rotationally invariant in the planes and shows an anisotropic direction along the normal c -axis, as displayed in Fig. 10

VI. TRANSPORT

In this section we calculate the optic and thermal conductivities of the SC phase in the clean limit. The transport calculation for a d -wave-order parameter with and without d -wave superconductivity has been done by Yang and Nayak.⁴¹ Here, we shall repeat this calculation for a CDW gap with nodes coexisting with a s -wave SC order parameter. We ignore the effects of scattering centers such as impurities and disorder from the CDW fluctuations motivated by two facts: (1) the TMD are very clean materials and (2) the extremely low temperatures where the SC phase appears in 2H-TaSe₂ ($T \leq 0.1$ K), where conventional thermal disorder in the CDW phase should play no relevant role in the transport.

The thermal current is defined by $\mathbf{j}^Q = \mathbf{j}^E - (\mu/e)\mathbf{j}$,³⁹ where \mathbf{j}^E is the energy current, \mathbf{j} is the electrical current, and μ is

the chemical potential. Experimental measurements of the thermal conductivity κ require zero electric current flow in the sample, and we may assume that $\mathbf{j}^Q = \mathbf{j}^E$. The Kubo formulas for frequency-dependent thermal conductivity $\kappa(\omega)$ and the optical conductivity $\sigma(\omega)$, are:³⁹

$$\kappa_{ij}(\omega) = -\frac{1}{\omega T} \lim_{q \rightarrow 0} \text{Im} \Pi_{ij}^{EE}(\mathbf{q}, \omega) + TS_{ij}^2(\omega) \sigma_{ij}(\omega), \quad (41)$$

$$\sigma_{ij}(\omega) = -\frac{1}{\omega} \lim_{q \rightarrow 0} \text{Im} \Pi_{ij}(\mathbf{q}, \omega), \quad (42)$$

where

$$S_{ij}(\omega) = -\frac{1}{T} \lim_{q \rightarrow 0} \left[\frac{\text{Im} \Pi_{ij}^E(\mathbf{q}, \omega)}{\text{Im} \Pi_{ij}(\mathbf{q}, \omega)} \right] \quad (43)$$

is the thermoelectric conductivity (also known as thermopower) $S = -\Delta V / \Delta T$, that measures the current voltage ΔV produced by a temperature gradient ΔT , and Π , Π^{EE} , and Π^E are, respectively, the electric, thermal, and thermoelectric current correlation functions, which we define in Appendix C. The second term in Eq. (40) guarantees the zero current flow condition to the charge carriers.

A. Optical conductivity

To incorporate the magnetic field into Hamiltonian (8), we proceed with the Peierls substitution $\mathbf{k} \rightarrow \mathbf{k} - (e/c)\tau_3 \mathbf{A}$. We assume that the vector potential $\mathbf{A}(\mathbf{k})$ is symmetric with respect to momentum inversion inside the nodal space. For this reason, we must use the τ_3 Pauli matrix, which operates in the usual Nambu space. Notice that a given Hamiltonian density for spin $\frac{1}{2}$ fermions in the form $\sum_{\sigma} f(\mathbf{k}) \psi_{\sigma}^{\dagger}(\mathbf{k}) \psi_{\sigma}(\mathbf{k})$ is equivalently written in the Nambu space as

$$[\psi_{\uparrow}^{\dagger}(\mathbf{k}), \psi_{\downarrow}^{\dagger}(-\mathbf{k})] \begin{pmatrix} f(\mathbf{k}) & 0 \\ 0 & -f(-\mathbf{k}) \end{pmatrix} \begin{pmatrix} \psi_{\uparrow}(\mathbf{k}) \\ \psi_{\downarrow}^{\dagger}(-\mathbf{k}) \end{pmatrix}.$$

The associated matrix above is clearly τ_3 if f is a symmetric function in k and τ_0 if f is antisymmetric. As the Dirac fermions dispersion is antisymmetric in the cone, we should be especially careful with the usual Peierls substitution, since it introduces an even term ($\propto \tau_3 \mathbf{A}$), which violates the odd symmetry of the zero-field dispersion dependence with k . For a given Hamiltonian in the general form

$$H = \sum_{\mathbf{k}} \epsilon_{\mathbf{k}} \Psi^{\dagger}(\mathbf{k}) \tau_0 \eta_i \Psi(\mathbf{k}),$$

the correct Peierls substitution involves the separation of symmetric (S) and antisymmetric (A) components in \mathbf{k} ,

$$\epsilon(\mathbf{k}) \tau_0 \rightarrow \epsilon^A \left(\mathbf{k} - \frac{e}{c} \tau_3 \mathbf{A} \right) \tau_0 + \epsilon^S \left(\mathbf{k} - \frac{e}{c} \tau_3 \mathbf{A} \right) \tau_3, \quad (44)$$

where

$$\epsilon^S \left(\mathbf{k} - \frac{e}{c} \tau_3 \mathbf{A} \right) = \frac{1}{2} \left[\epsilon \left(\mathbf{k} - \frac{e}{c} \tau_3 \mathbf{A} \right) + \epsilon \left(-\mathbf{k} - \frac{e}{c} \tau_3 \mathbf{A} \right) \right]$$

$$\epsilon^A \left(\mathbf{k} - \frac{e}{c} \tau_3 \mathbf{A} \right) = \frac{1}{2} \left[\epsilon \left(\mathbf{k} - \frac{e}{c} \tau_3 \mathbf{A} \right) - \epsilon \left(-\mathbf{k} - \frac{e}{c} \tau_3 \mathbf{A} \right) \right].$$

Applying this procedure to the Hamiltonian (8), it is easy to see that the magnetic part of the Hamiltonian is

$$H_B = -\Psi^{\dagger}(\mathbf{k}) \left[v_F \frac{e}{c} A_{\perp} \tau_0 \eta_3 + v_{\Delta} \frac{e}{c} A_{\parallel} \tau_0 \eta_1 \right] \Psi(\mathbf{k}),$$

written in terms of τ_0 instead of τ_3 , as one could naively expect from the straight substitution $\mathbf{k} \rightarrow \mathbf{k} - (e/c)\tau_3 \mathbf{A}$.

The current density operator $\mathbf{j}(\mathbf{k}) = -c \nabla_{\mathbf{A}} H$ is given by

$$\mathbf{j}(\mathbf{k}) = \Psi^{\dagger}(\mathbf{k}) [v_F e \tau_0 \eta_3 \hat{\mathbf{e}}_{\perp} + v_{\Delta} e \tau_0 \eta_1 \hat{\mathbf{e}}_{\parallel}] \Psi(\mathbf{k}). \quad (45)$$

The current-current density correlation function defined in Appendix C is given by:

$$\Pi_{\perp}(\mathbf{q}, i\omega) = \frac{v_F^2 e^2}{\beta} \text{Tr} \sum_{\mathbf{k}, \omega_n} \vec{G}_{+} \tau_0 \eta_3 \vec{G}_{-} \tau_0 \eta_3,$$

$$\Pi_{\parallel}(\mathbf{q}, i\omega) = \frac{v_{\Delta}^2 e^2}{\beta} \text{Tr} \sum_{\mathbf{k}, \omega_n} \vec{G}_{+} \tau_0 \eta_1 \vec{G}_{-} \tau_0 \eta_1,$$

where \perp and \parallel are the normal and parallel directions to the Fermi surface for a given node (see Fig. 2). Applying the Kubo formula (41) to the imaginary part of the correlation functions above, we find that the optical conductivity is separated into two parts: the Drude term

$$\sigma_{\perp}^{DC}(\omega) = -\frac{v_F e^2}{2v_{\Delta}} \delta(\omega) \sum_{\sigma'=\pm 1} \int_0^{\alpha} d\epsilon \epsilon \left(1 - \frac{\Delta_s^2}{E_{\sigma'\mu}^2} \right) \frac{\partial n(E_{\sigma'\mu})}{\partial E_{\sigma'\mu}} \quad (46)$$

and an extra term due to the interband excitations of the Dirac fermions,

$$\begin{aligned} \sigma_{\perp}^{AC}(\omega) &= \frac{2v_F e^2 \Delta_s^2}{v_{\Delta} \omega^2} \left[n \left(-\frac{|\omega|}{2} \right) - n \left(\frac{|\omega|}{2} \right) \right] \\ &\times \theta(|\omega| - 2\sqrt{\mu^2 + \Delta_s^2}) + \frac{v_F e^2}{2v_{\Delta}} \omega \nu_0 \left(1 - \frac{4\mu^2}{\omega^2} \right) \\ &\times \left\{ \theta \left(|\mu| - \frac{|\omega|}{2} \right) \frac{1}{\Theta_{-}} [n(E_{0,|\mu|}) - n(E_{0,-|\mu|})] \right. \\ &\left. - \theta \left(\frac{|\omega|}{2} - \sqrt{\mu^2 + \Delta_s^2} \right) \frac{1}{\Theta_{+}} [n(E_{0,\mu}) - n(-E_{0,-\mu})] \right\} \\ &\xrightarrow{T \rightarrow 0} \frac{v_F e^2}{2v_{\Delta}} \left[\left(1 - \frac{4\mu^2}{\omega^2} \right) \frac{\omega \nu_0}{\Theta_{+}} + \frac{4\Delta_0^2}{\omega^2} \right] \\ &\times \theta(|\omega| - 2\sqrt{\mu^2 + \Delta_s^2}), \end{aligned} \quad (47)$$

where

$$\nu_0 \equiv \frac{\omega}{2} \sqrt{1 - \frac{4\Delta_s^2}{\omega^2 - 4\mu^2}} \quad (48)$$

and

$$\Theta_{\pm} = (|\nu_0| - \mu) E_{0,\mu} \pm (|\nu_0| + \mu) E_{0,-\mu}$$

with $E_{0,\pm\mu}^2 = (|\nu_0| \pm \mu)^2 + \Delta_s^2$. In order to calculate the parallel component σ_{\parallel} we just have to exchange v_F and v_{Δ} . For $\omega = 0$, the interband conductivity is given by:

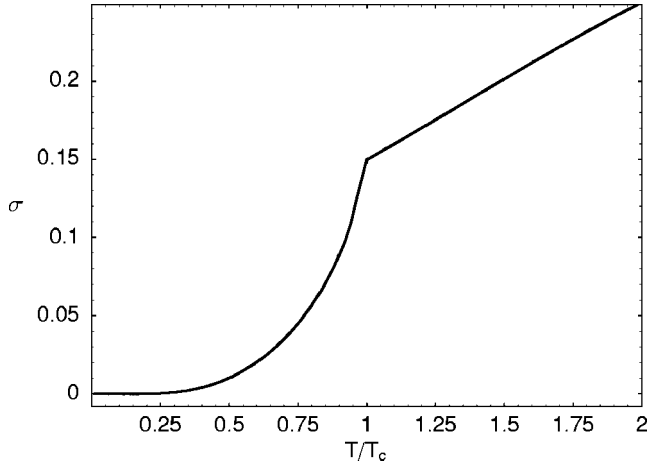


FIG. 11. Temperature dependence of the Drude conductivity integrated in ω , for $g/g_c=1.1$ and $\mu/\alpha=0.1$. σ in units of $v_F e^2 \alpha / (2v_\Delta)$.

$$\sigma_{\perp}^{AC}(\omega) = \frac{e^2 v_F}{2v_\Delta} \left(1 + \frac{4\Delta_s^2}{\omega^2} \right) \left| 1 - 2n\left(\frac{\omega}{2}\right) \right| \theta(|\omega| - 2\Delta_s). \quad (49)$$

The conductivity (46) is considerably simpler in the normal CDW phase. Setting the gap Δ_s to zero, we have $v_0 \rightarrow \omega/2$ and $E_{0,\pm\mu} \rightarrow |\omega|/2 \pm \mu$, leading to

$$\begin{aligned} \sigma_{\perp CDW}^{AC}(\omega) &= \frac{v_F e^2}{2v_\Delta} \left[n\left(-\frac{|\omega|}{2} + \mu\right) - n\left(\frac{|\omega|}{2} + \mu\right) \right] \\ &\xrightarrow{T \rightarrow 0} \frac{v_F e^2}{2v_\Delta} \theta\left(\frac{|\omega|}{2} - |\mu|\right). \end{aligned} \quad (50)$$

Analogously, the Drude part of the conductivity becomes

$$\begin{aligned} \sigma_{\perp CDW}^{DC}(\omega) &= \frac{v_F e^2 \beta}{8v_\Delta} \delta(\omega) \sum_{\sigma'=\pm 1} \int_0^\alpha d\epsilon \epsilon \operatorname{sech}^2\left(\beta \frac{\epsilon + \sigma' \mu}{2}\right) \\ &\xrightarrow{T \rightarrow 0} \frac{v_F e^2}{2v_\Delta} \delta(\omega) \times \begin{cases} \ln(2) \frac{2}{\beta}, & \text{for } \mu = 0, \\ |\mu|, & \text{for } \mu \neq 0. \end{cases} \end{aligned} \quad (51)$$

Notice that in the absence of SC we find that $\sigma^{DC}(T \rightarrow 0)$ is constant and proportional to μ . In the SC case, Eq. (45) shows that $\sigma^{DC}(T \rightarrow 0)$ vanishes independently of the pocket size (as shown in Fig. 11). The presence of a Drude conductivity $\sigma^{DC} \propto \delta(\omega)$, results from an infinite electron mean free path due to the absence of scattering centers. If we consider that the electrons in TaSe₂ have a finite scattering rate $\Gamma = 1/\tau(\omega)$,³⁷ the Drude peak will be broadened around $\omega = 0$. The normal transport in the presence of an order parameter with nodes (such as the CDW, in our case) in the dirty limit is given in Ref. 41.

Photon absorption involves quasiparticle excitations and results in the formation of in-phase currents with the electric field.⁴² The absorption rate is therefore proportional to the

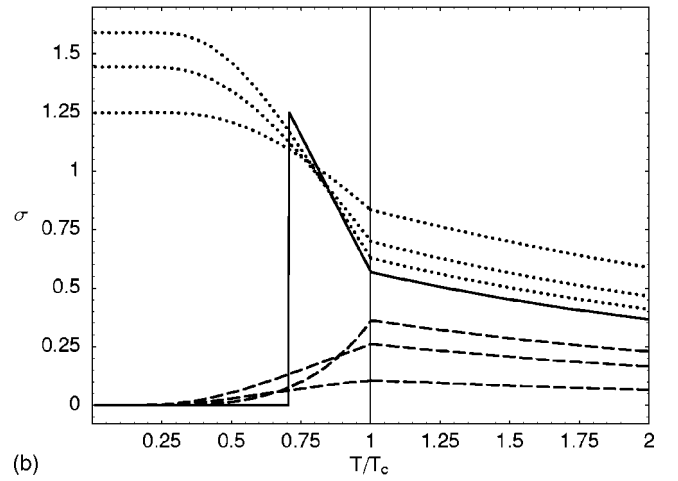
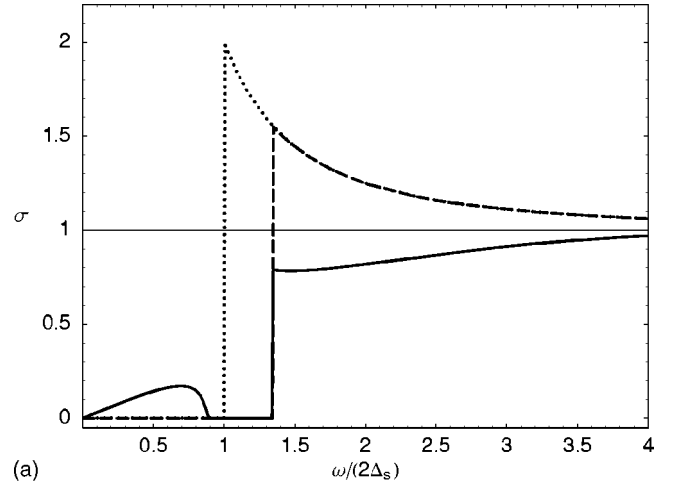


FIG. 12. Top: optical conductivity σ_{\perp} vs frequency. For $|\mu|/(2\Delta_s)=0.9$: dashed line ($T=0$) and solid [$k_B T/(2\Delta_s)=1.2$]; dotted line: $\mu=0$ and $T=0$. Bottom: optical conductivity σ_{\perp} vs temperature, for $g/g_c=1.1$ and $|\mu|/\alpha=0.1$. Dashed lines: $0.4\Delta_0\mu < \omega < 1.4\Delta_0\mu$; solid: $\omega=2.3\Delta_0\mu$; dotted: $2.8\Delta_0\mu < \omega < 4\Delta_0\mu$. In both plots, σ is in units of $v_F e^2 / (2v_\Delta)$.

real part of the conductivity. In conventional superconductors, there is no absorption at $T=0$ in the infrared region, where the photons with energy $\omega < 2\Delta_s$ cannot break a Cooper pair. At finite temperature, the excitation channels are gradually recovered and photons with energy smaller than $2\Delta_s$ have a finite probability of been absorbed. We should stress that the coherence factors in those superconductors (say, BCS type) are finite only in the dirty case, where the processes conserve energy but do not conserve momentum. The first important distinction of the traditional superconductors to the Dirac fermion ones is in the presence of *two* bands, resembling the spectrum of small gap semiconductors (see Fig. 3). In the nodal liquid superconductor, made out of Cooper pairs of Dirac fermions, the clean limit absorption process comprehends the excitation of an electron from the lower to the upper band, transferring energy equal to the photon energy ω but with no momentum transfer. In the situation where the lower band is completely filled ($\mu=0$), there are no thermal channels of quasiparticle excitations (since

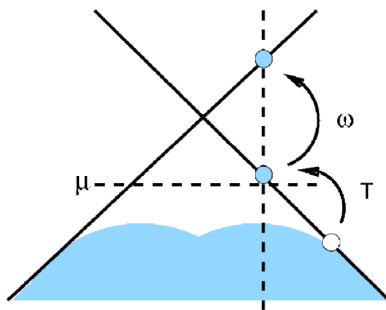


FIG. 13. Schematic representation of the photon absorption process in the channel of thermal excitations of the condensate, within the absorption window $|\omega| < 2|\mu|$ of the holelike branch (see Fig. 3). ω is the photon frequency, T represents the thermal excitations, and μ indicates the Fermi level.

the thermally excited electrons occupy the upper band, where there is no absorption due to momentum conservation) and the photon is absorbed only when its energy is sufficient to break a pair ($|\omega| > 2\Delta_s$), producing quasiparticle excitations directly from the condensate (pair-breaking channels). When the system exhibits particle-hole symmetry, the clean limit absorption is totally independent of the temperature in the infrared, for $\omega < 2\Delta_s$.

The second important distinction is that the optical conductivity shows an anomalous absorption edge in $\omega = 2\sqrt{\mu^2 + \Delta_s^2}$ (see Fig. 12). This energy corresponds to the optical gap of the two bands shown in Fig. 3. The presence of the edge is a consequence of the broken lattice inversion symmetry in the CDW distorted phase, which affects the coherence factors of the infrared conductivity (in our case, type I, similar to the charge interactions). When the particle-hole symmetry is lost by shifting the chemical potential from the vertex of the Dirac cone, new thermal channels of quasiparticle excitations emerge, giving rise to an absorption peak in the infrared. To see this effect, we illustrate in Fig. 13 the thermal excitation process of the holelike branch, where photons with energies smaller than $2|\mu|$ are able to promote the thermally excited electrons occupying the empty states in the top of the lower band to the upper band. As in the case of superfluid He^3 , the superconductor is an electronic liquid composed of two “fluids,” where there is a one-to-one correspondence between the excited states in the SC and in the normal phases. The thermal excitations promote electrons from the condensate to the empty states above the pocket Fermi surface of the holelike branch. The optical channels of absorption through the thermally excited electrons are therefore limited to the window $|\omega| \leq 2|\mu|$ (in the clean limit), as shown in Figs. 12 (top) and 13.

The temperature dependence of the optical conductivity, displayed in Fig. 12 (bottom), shows a clear distinction between the two absorption channels. The dashed lines represent the thermal channels, which vanish at $T=0$. The dotted lines indicate the pair-breaking channels. These channels depend on the number of electrons in the condensate and are more effective as the temperature is reduced. The solid line in the same figure represents a pair-breaking channel which is abruptly suppressed by lowering the temperature. This is understood by noting that the optical gap $2\sqrt{\mu^2 + \Delta_s^2(T)}$ [see

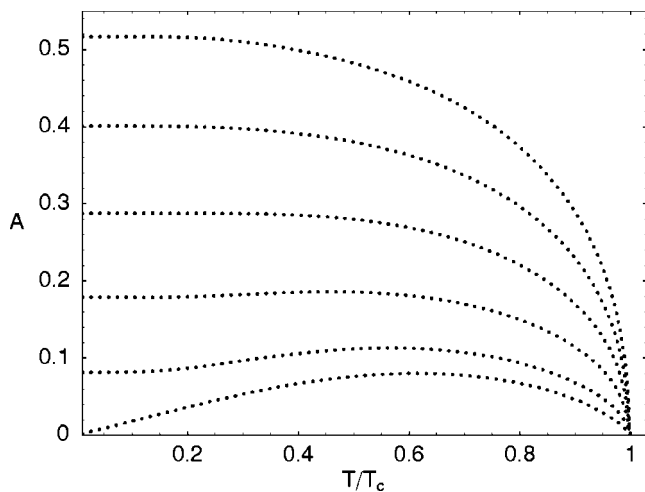


FIG. 14. Meissner spectral weight A as a function of temperature. Curves drawn for $0 \leq |\mu|/\alpha \leq 0.15$, from the bottom to the top, in fixed intervals of 0.03. A in units of $v_F e^2 \alpha / (2v_\Delta)$, with $g/g_c = 1.1$.

Fig. 12 (top)] displaces the absorption edge towards the ultraviolet as the temperature is reduced. In this situation, we expect that some of the absorption channels at a given energy slightly to the right of the edge will be abruptly suppressed if the temperature is sufficiently reduced, i.e., if the edge is sufficiently displaced to the right in Fig. 12 (bottom).

1. Spectral weight

According to the f sum rule one should have

$$\int_0^\infty \sigma(\omega) d\omega = \frac{\pi n e^2}{2m}, \quad (52)$$

and therefore, the area “under” the curves $\sigma^{DC} + \sigma^{AC}$ is conserved in the normal and in the SC phases. In the SC phase, however, there is a “missing” area in comparison to the normal phase. The difference between the two areas corresponds to the $\omega=0$ spectral weight, responsible for the diamagnetic supercurrents in the Meissner effect.³³ This part of the spectral weight (which properly defines a superconductor) depends on a different order of limits between ω and q , and does not appear explicitly in the calculation. Thus, a required condition for superconductivity is

$$\int_0^\infty [\sigma_s^{DC}(\omega) + \sigma_s^{AC}(\omega)] d\omega < \int_0^\infty [\sigma_n^{DC}(\omega) + \sigma_n^{AC}(\omega)] d\omega.$$

From now on, we call the difference between the n and s areas the Meissner spectral weight.

It is not difficult to see that for $\mu=0$ at zero temperature we have $\sigma_s^{DC} = \sigma_n^{DC} = 0$, and that the curves in the AC sector have *exactly* the same area. This behavior is depicted in Fig. 14 for different values of μ , showing an anomalous suppression of the Meissner spectral weight at low temperatures for small μ . A superficial analysis would indicate that there is no spectral weight due to the condensate and therefore the

superconductivity is not stable. This analysis, however, is incompatible with the thermodynamic verification that there is a finite zero-temperature critical field $H_c(0)$ (see Fig. 7), resulting in a finite condensation energy.

The origin of the problem has connections with the spectral weight shift from the high- to the low-energy states of the band as the temperature is reduced, which has been observed experimentally in the crystal of TaSe₂.²² In this compound, part of the spectral weight around 60 meV (\sim of the order of the cone cutoff) at 300 K is displaced towards the infrared at temperatures of the order of the SC phase transition. Apparently, the opening of the gap attracts states beyond the cone approximation. In lowest order, the nonlinear states in the CDW spectrum yield $\epsilon_{\mathbf{k}} \propto [k - (e/c)A]^2$. These states are the only ones that contribute to the diamagnetism, which results from terms $\propto A^2$ in the energy. We conclude that the cone approximation excludes the ‘‘diamagnetic’’ states of the band, and for this reason the f -sum rule is not able to correctly incorporate the diamagnetic spectral weight, especially at low temperature, where the contribution of the high-energy states is more pronounced. The zero-field properties which are not directly related to the Meissner effect, however, are not so sensitive to the absence of the high-energy states and give satisfactory results within the cone approximation. This analysis is confirmed later in Sec. VII, when we discuss the Meissner effect in the London limit.

B. Thermal conductivity

The energy current is a conserved quantity defined by the nondiagonal components of the momentum-energy tensor T_{0i}^j , defined as⁴³

$$T_{\nu}^{\mu} \equiv \frac{\partial \mathcal{L}}{\partial (\partial_{\mu} \Psi)} \partial_{\nu} \Psi - \mathcal{L} \delta_{\nu}^{\mu}. \quad (53)$$

According to the usual relation $H = [\partial \mathcal{L} / \partial (\partial_0 \Psi)] \partial_0 \Psi - \mathcal{L}$, the Lagrangian associated to the Hamiltonian (8) in the real space representation is

$$\begin{aligned} \mathcal{L} = & \Psi^{\dagger}(x) [ic\tau_3\eta_0\partial_0 - iv_F\tau_0\eta_3\partial_3 - iv_{\Delta}\tau_0\eta_1\partial_1 - \Delta_s\tau_1\eta_2 \\ & + \mu\tau_3\eta_0] \Psi(x), \end{aligned} \quad (54)$$

where $c\partial_0 \equiv ic\partial_{\tau}$ with τ as the imaginary time. The conserved energy current $\mathbf{j}^E(x) = cT_0^i$ gives

$$\mathbf{j}^E(x) = \frac{\partial \mathcal{L}}{\partial (\partial_i \Psi)} c\partial_0 \Psi = \Psi^{\dagger}(x) [v_F\tau_0\eta_3\hat{\mathbf{e}}_{\perp} + v_{\Delta}\tau_0\eta_1\hat{\mathbf{e}}_{\parallel}] \partial_{\tau} \Psi(x)$$

or, equivalently,

$$\begin{aligned} \mathbf{j}^E(\mathbf{q}, \tau) = & - \sum_{\mathbf{k}} \Psi^{\dagger}(\mathbf{k} - \mathbf{q}/2, \tau) [v_F\tau_0\eta_3\hat{\mathbf{e}}_{\perp} \\ & + v_{\Delta}\tau_0\eta_1\hat{\mathbf{e}}_{\parallel}] \vec{\omega}_{\mathbf{k}+\mathbf{q}/2} \Psi(\mathbf{k} + \mathbf{q}/2, \tau), \end{aligned} \quad (55)$$

where the time evolution of the Dirac fermions Ψ is

$$\Psi(\mathbf{q}, \tau) = e^{-\tau \vec{\omega}_{\mathbf{q}}} \Psi(\mathbf{q}),$$

with $\vec{\omega}$ defined in Eq. (8).

We are interested in the diagonal components of the current-current polarizations $\Pi_{11}^{EE} \equiv \Pi_{\perp}^{EE}$ and $\Pi_{11}^E \equiv \Pi_{\perp}^E$ given by:

$$\Pi_{\perp}^{EE}(\mathbf{q}, i\omega) = \frac{v_F^2}{\beta} \text{Tr} \sum_{\mathbf{k}, \omega_n} \vec{G}_{+} \tau_0 \eta_3 \vec{\omega}_{+} \vec{G}_{-} \tau_0 \eta_3 \vec{\omega}_{-},$$

$$\Pi_{\perp}^E(\mathbf{q}, i\omega) = \frac{v_F e}{\beta} \text{Tr} \sum_{\mathbf{k}, \omega_n} \vec{G}_{+} \tau_0 \eta_3 \vec{\omega}_{+} \vec{G}_{-} \tau_0 \eta_3.$$

We find that

$$\begin{aligned} \text{Im} \Pi_{\perp}^{EE}(0, \omega) = & \frac{v_F \omega}{2v_{\Delta}} \delta(\omega) \sum_{\sigma'=\pm 1} \int_0^{\alpha} d\epsilon \epsilon E_{\sigma'\mu}^2 \left(1 - \frac{\Delta_s^2}{E_{\sigma'\mu}^2} \right) \frac{\partial n(E_{\sigma'\mu})}{E_{\sigma'\mu}} - \frac{v_F}{2v_{\Delta}} \omega^2 \nu_0 \left(1 - \frac{4\mu^2}{\omega^2} \right) E_{0,\mu} E_{0,-\mu} \\ & \times \left\{ \theta \left(|\mu| - \frac{|\omega|}{2} \right) \frac{1}{\Theta_{-}} [n(E_{0,|\mu|}) - n(E_{0,-|\mu|})] + \theta \left(\frac{|\omega|}{2} - \sqrt{\mu^2 + \Delta_s^2} \right) \frac{1}{\Theta_{+}} [n(E_{0,\mu}) - n(-E_{0,-\mu})] \right\} \\ & + \frac{v_F \omega}{2v_{\Delta}} \Delta_s^2 \left[n \left(-\frac{|\omega|}{2} \right) - n \left(\frac{|\omega|}{2} \right) \right] \theta(|\omega| - 2\sqrt{\mu^2 + \Delta_s^2}), \end{aligned} \quad (56)$$

and

$$\begin{aligned} \text{Im} \Pi_{\perp}^E(0, \omega) = & \frac{v_F e}{4v_{\Delta}} \omega^2 |\nu_0| \left(1 - \frac{4\mu^2}{\omega^2} \right) \left\{ \theta \left(|\mu| - \frac{|\omega|}{2} \right) [E_{0,\mu} - E_{0,-\mu}] \frac{1}{\Theta_{-}} [n(E_{0,\mu}) - n(E_{0,-\mu})] \right. \\ & \left. - \theta \left(\frac{|\omega|}{2} - \sqrt{\mu^2 + \Delta_s^2} \right) [E_{0,\mu} + E_{0,-\mu}] \frac{1}{\Theta_{+}} [n(E_{0,\mu}) - n(-E_{0,-\mu})] \right\} \\ & + \frac{v_F e}{v_{\Delta}} \Delta_s^2 \left[n \left(-\frac{|\omega|}{2} \right) - n \left(\frac{|\omega|}{2} \right) \right] \theta(|\omega| - 2\sqrt{\mu^2 + \Delta_s^2}). \end{aligned} \quad (57)$$

where ν_0 and $E_{0,\sigma\mu}$ are defined as in Eq. (47). In contrast to the thermal polarization, the thermoelectric one does not have a Drude part. The thermal conductivity follows from a straightforward substitution of the previous results (46), (55), and (56) into the Kubo formula (40).

Let us analyze these results for $\mu=0$. We have

$$\begin{aligned} \frac{1}{\omega} \text{Im} \Pi_{\perp}^{EE}(0, \omega) &= \frac{v_F}{v_{\Delta}} \delta(\omega) \int_{\Delta_s}^{E_{\Lambda}} dE^3 \left(1 - \frac{\Delta_s^2}{E^2} \right) \\ &\times \frac{\partial n(E)}{\partial E} + \frac{v_F}{2v_{\Delta}} \left(\frac{\omega}{2} \right)^2 \left(1 + \frac{4\Delta_s^2}{\omega^2} \right) \\ &\times \left[1 - 2n\left(\frac{|\omega|}{2}\right) \right] \theta(|\omega| - 2\Delta_s) \quad (58) \end{aligned}$$

and

$$\begin{aligned} \frac{1}{\omega} \text{Im} \Pi_{\perp}^E(0, \omega) &= \frac{ev_F}{2v_{\Delta}} \frac{\omega}{2} \left(1 + \frac{4\Delta_s^2}{\omega^2} \right) \\ &\times \left[1 - 2n\left(\frac{|\omega|}{2}\right) \right] \theta(|\omega| - 2\Delta_s). \quad (59) \end{aligned}$$

Replacing Eqs. (48) and (58) into Eq. (42), the $\mu=0$ thermopower yields

$$S_{\perp} = - \frac{1}{T} \frac{\text{Im} \Pi_{\perp}^E(0, \omega)}{\text{Im} \Pi_{\perp}^{EE}(0, \omega)} = \frac{\omega}{2eT}. \quad (60)$$

Substituting Eqs. (48), (57), and (59) into Eq. (40), we find that the only contribution comes from the Drude term

$$\kappa_{\perp}(\omega) = - \frac{v_F}{v_{\Delta} T} \delta(\omega) \int_{\Delta_s}^{E_{\Lambda}} dE E^3 \left(1 - \frac{\Delta_s^2}{E^2} \right) \frac{\partial n(E)}{\partial E}, \quad (61)$$

where $\kappa^{AC}=0$ for zero μ . When the system exhibits particle-hole symmetry, the exact cancellation of the interband contributions to the thermal conductivity is due to the fact that the total heat carried by the particle-hole pair is zero. The argument is the following:⁴¹ the interband excitation process involves the annihilation of an electron with negative energy in the lower band, and the creation of a particle with positive energy $-E_{\mathbf{k}} + \omega = +E_{\mathbf{k}}$ in the upper band, where ω is the photon energy and $-E_{\mathbf{k}}$ is the energy of the annihilated electron. Destroying a particle with negative energy, momentum \mathbf{k} and charge e is equivalent to create a hole with momentum $-\mathbf{k}$ and charge $-e$ at the energy cost $+E_{\mathbf{k}}$. The energy current carried by the quasiparticle formed by the particle-hole pair is $\mathbf{k}E_{\mathbf{k}} + (-\mathbf{k})(E_{\mathbf{k}}) = 0$. On the other hand, the charge current is finite, $\mathbf{k}e + (-\mathbf{k})(-e) = 2e\mathbf{k}$, explaining why the quasiparticles are able to transport charge but not heat when the pocket is absent.

When the particle-hole symmetry is lost, the thermal current due to the pair breaking channels is equal to $E_{\mathbf{k},\mu}(\mathbf{k}) + (E_{\mathbf{k},-\mu})(-\mathbf{k})$, or equivalently to $2\mu\mathbf{k}$ in the normal CDW phase, when the ground-state electrons are promoted to the upper band. As a second effect, the thermal channels of quasiparticle production give rise to an infrared peak for $|\omega| < 2|\mu|$ as shown in Fig. 15 (top), analogously to the optical conductivity. In contrast to the charge transport, how-

ever, the amount of heat carried by the quasiparticles is of the order of the pocket energy and vanishes at $\mu=0$. The temperature dependence of κ is shown in Fig. 15 (bottom). The solid lines represent the thermal channels of quasiparticle excitation, while the dotted lines indicate the pair breaking channels. As in the case of the optical conductivity, some of the latter channels which are slightly above the optical gap energy $\omega_0 = 2\sqrt{\mu^2 + \Delta_s^2}$ are suppressed at low temperatures (see Fig. 15). At $T=0$ the thermal conductivity is zero for $|\omega| < \omega_0$, and infinity for $|\omega| > \omega_0$.

Let us verify the normal CDW properties ($\Delta_s=0$) in the transport. The thermoelectric spectral function (56) is given by

$$\frac{1}{\omega} \text{Im} \Pi_{\perp}^{E}_{\text{CDW}}(0, \omega) = \frac{v_F e}{2v_{\Delta}} \frac{\omega}{2} \left[n\left(-\frac{|\omega|}{2} + \mu\right) - n\left(\frac{|\omega|}{2} + \mu\right) \right].$$

Comparing the expression above with the optical conductivity of the normal phase (49), the thermoelectric coefficient yields

$$S_{\perp \text{CDW}}(\omega) = \frac{\omega}{2eT},$$

as in the SC particle-hole symmetric case (59). Returning to Eq. (55), and setting $\Delta_s=0$, we have

$$\begin{aligned} \frac{1}{\omega} \text{Im} \Pi_{\perp}^{EE}_{\text{CDW}}(0, \omega) &= \frac{v_F}{2v_{\Delta}} \left[\left(\frac{\omega}{2} \right)^2 - \mu^2 \right] \\ &\times \left[n\left(-\frac{|\omega|}{2} + \mu\right) - n\left(\frac{|\omega|}{2} + \mu\right) \right]. \end{aligned}$$

The thermal conductivity therefore yields:

$$\kappa_{\text{CDW}}(\omega) = \kappa_{\text{CDW}}^{\text{DC}}(\omega) + \kappa_{\text{CDW}}^{\text{AC}}(\omega),$$

where

$$\begin{aligned} \kappa_{\perp \text{CDW}}^{\text{DC}}(\omega) &= - \frac{v_F \delta(\omega)}{2v_{\Delta} T} \sum_{\sigma'=\pm 1} \int_0^{\alpha} d\epsilon \epsilon E_{\sigma'\mu}^2 \frac{\partial n(E_{\sigma'\mu})}{E_{\sigma'\mu}} \\ &\xrightarrow{T \rightarrow 0} \frac{v_F k_B}{2v_{\Delta} \beta^2} \delta(\omega) \begin{cases} 9\zeta(3), \text{ for } \mu = 0 \\ \frac{\pi^2}{3} \beta |\mu|, \text{ for } \mu \neq 0 \end{cases}, \quad (62) \end{aligned}$$

and

$$\begin{aligned} \kappa_{\perp \text{CDW}}^{\text{AC}}(\omega) &= \mu^2 \frac{v_F}{2v_{\Delta} T} \left[n\left(-\frac{|\omega|}{2} + \mu\right) - n\left(\frac{|\omega|}{2} + \mu\right) \right] \\ &\xrightarrow{T \rightarrow 0} \mu^2 \frac{v_F}{2v_{\Delta} T} \theta\left(\frac{|\omega|}{2} - |\mu|\right). \quad (63) \end{aligned}$$

The verification of the Wiedmann-Franz (WF) law can be done in two cases. For $\mu=0$, despite the optical conductivity is dominated in the low temperature region by the interband conductivity

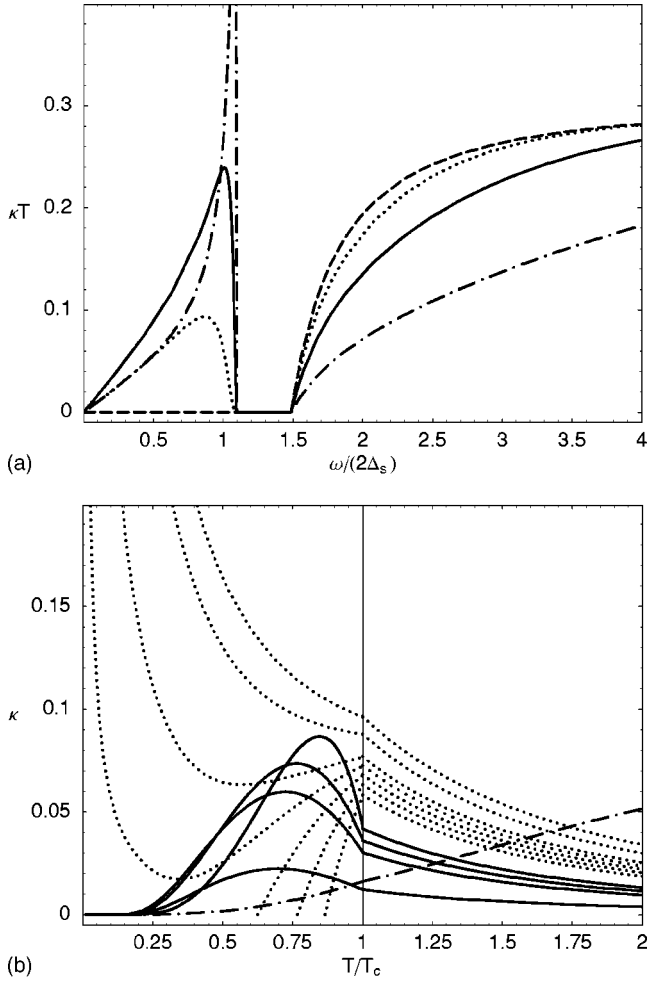


FIG. 15. Top: thermal conductivity $\times T$ vs frequency. κT is in units of $(2v_F/v_\Delta)\Delta_s^2$ and ω in units of $2\Delta_s$, with $\mu=2.2\Delta_s$. Dashed line: $T \rightarrow 0$ limit; dotted ($k_B T = \frac{1}{2}\Delta_s$); solid ($k_B T = \Delta_s$); dot-dashed: ($k_B T = \frac{5}{2}\Delta_s$). Below: thermal conductivity dependency with temperature. We have set κ in units of $v_F k_B \alpha / (2v_\Delta)$, $g/g_c = 1.1$, and $|\mu/\alpha| = 0.1$. Solid lines: $0.4\Delta_{0\mu} < \omega < 1.4\Delta_{0\mu}$; dotted: $2\Delta_{0\mu} < \omega < 4\Delta_{0\mu}$. The dot-dashed line is the Drude thermal conductivity integrated in ω with units of $\frac{1}{5}v_F k_B \alpha^2 / (2v_\Delta)$.

$$\sigma_{\perp \text{CDW}}(\omega, T \rightarrow 0) = \frac{v_F e^2}{2v_\Delta} \tanh\left(\frac{\beta\omega}{4}\right) + \ln(2) \frac{v_F e^2}{v_\Delta \beta} \delta(\omega), \quad (64)$$

the $\omega/(k_B T) \ll 1$ limit is dominated by the Drude part. Comparing the expression above with Eq. (61) for $\mu=0$, we see that the CDW phase obeys the temperature dependence of the WF law

$$\lim_{T \rightarrow 0} \frac{\kappa_{\text{CDW}}(0, T)}{T \sigma_{\text{CDW}}(0, T)} = \frac{9\zeta(3)}{2 \ln(2)} \left(\frac{k_B}{e}\right)^2, \quad (65)$$

but with a particular numerical constant $9\zeta(3)/[2 \ln(2)] \approx 7.8$. Note that the order of the limits is essential, otherwise, σ_{CDW} is dominated by the interband term in the $\omega/(k_B T) \gg 1$ limit

$$\lim_{\omega \rightarrow 0} \sigma_{\text{CDW}}(\omega, 0) = \frac{v_F e^2}{2v_\Delta},$$

violating the WF law. We should stress, however, that this relation is typically valid in the dc limit $\omega \rightarrow 0$, which is well defined for $\beta\omega \ll 1$ but not for $\beta\omega \gg 1$. This is easily seen by noticing that at $T=0$ the quasiparticle excitation energy ω do not have a scale and the ac and dc sectors cannot be distinguished from one another.

For finite μ , it is immediate to check that the WF relation is verified exactly as in a metal,

$$\lim_{T \rightarrow 0} \frac{\kappa_{\text{CDW}}(0, T)}{T \sigma_{\text{CDW}}(0, T)} = \frac{\pi^2}{3} \left(\frac{k_B}{e}\right)^2.$$

VII. MEISSNER EFFECT

The nonlocal electrodynamic is described in the London limit where the vector potential function $\mathbf{A}(\mathbf{k}) \rightarrow \mathbf{A}_0 = \text{const.}$, under the assumption that the field variations are slow in comparison to the coherence length ξ . In this limit, the current \mathbf{j} and the vector potential obey the London equation

$$\langle j_i \rangle = j_i^{c.m.} + Q_{ij} A_j,$$

valid in the Coulomb gauge $\mathbf{k} \cdot \mathbf{A} = 0$, where $\mathbf{j}^{c.m.}$ is the current due to the momentum of the pair center-of-mass. For all purposes, we neglect this effect and consider only the response to the magnetic field.

To calculate the London kernel Q_{ij} , instead of writing the current density operator (44), we propose a more general calculation, extending the CDW band beyond the cone approximation. As in Sec. II, we start from a CDW Hamiltonian written in terms of an extended band

$$H_{\text{CDW}} = \sum_{\mathbf{k}, \sigma} \Psi_\sigma^\dagger(\mathbf{k}) [\epsilon_{\mathbf{k}} \eta_3 + \Delta_{c\mathbf{k}} \eta_1] \Psi_\sigma(\mathbf{k}), \quad (66)$$

where $\epsilon_{\mathbf{k}}$ and $\Delta_{c\mathbf{k}}$ are *any* antisymmetric functions of \mathbf{k} with respect to a given Fermi surface node.

Introducing the magnetic field through the modified Peierls substitution (43), the series expansion of $\epsilon[\mathbf{k} - (e/c)\tau_3 \mathbf{A}]$ in powers of \mathbf{A} is separated into symmetric and antisymmetric terms in k ,

$$\begin{aligned} \epsilon\left(\mathbf{k} - \frac{e}{c}\tau_3 \mathbf{A}\right) &= [\epsilon^{(0)}(\mathbf{k}) + \epsilon^{(2)}(\mathbf{k}) + \dots] \tau_0 \\ &\quad + [\epsilon^{(1)}(\mathbf{k}) + \epsilon^{(3)}(\mathbf{k}) + \dots] \tau_3 \\ &= \left[\epsilon_{\mathbf{k}} - \frac{e}{c} A_i \partial^i \epsilon_{\mathbf{k}} + \frac{1}{2} \left(\frac{e}{c}\right)^2 A_i A_j \partial^i \partial^j \epsilon_{\mathbf{k}} \right] \tau_0, \end{aligned}$$

up to second order in \mathbf{A} , where $\partial^i \equiv \partial/\partial k_i$ defines the momentum derivatives and repeated indexes are to be summed. The same applies to $\Delta_c[\mathbf{k} - (e/c)\tau_3 \mathbf{A}]$. Using the abbreviation $\tilde{\mathbf{k}} \equiv \mathbf{k} - (e/c)\tau_3 \mathbf{A}$, the Hamiltonian of the CDW+SC phase with an external magnetic field is

$$H = \sum_{\mathbf{k}} \Psi^\dagger(\tilde{\mathbf{k}}) [\tilde{\epsilon}_{\tilde{\mathbf{k}}} \tau_0 \eta_3 + \Delta_{c\tilde{\mathbf{k}}} \tau_0 \eta_1 + \Delta_s \tau_1 \eta_2 - \mu \tau_3 \eta_0] \Psi(\tilde{\mathbf{k}}).$$

The current density operator $\vec{j}_i(\mathbf{k}) = -c \nabla_{\mathbf{A}} H$ gives

$$\begin{aligned} \vec{j}_i(\mathbf{k}) = & \Psi^\dagger(\tilde{\mathbf{k}}) \left[e \left(\partial^i \epsilon_{\mathbf{k}} - \frac{e}{c} A_j \partial^j \partial^i \epsilon_{\mathbf{k}} \right) \tau_0 \eta_3 \right. \\ & \left. + e \left(\partial^j \Delta_{c\mathbf{k}} - \frac{e}{c} A_j \partial^j \Delta_{c\mathbf{k}} \right) \tau_0 \eta_1 \right] \Psi_{\tilde{\mathbf{k}}}. \end{aligned}$$

We calculate the expectation value $\langle \vec{j} \rangle$ up to first order in \mathbf{A} (see details in Appendix E), and find that the London kernel reads

$$\begin{aligned} Q_{ij} = & \frac{e^2}{c} \sum_{\mathbf{k}} \sum_{\sigma=\pm 1} \left\{ \frac{\beta}{2} [(\partial_i \epsilon_{\mathbf{k}})(\partial_j \epsilon_{\mathbf{k}}) + (\partial_i \Delta_{c\mathbf{k}})(\partial_j \Delta_{c\mathbf{k}})] \right. \\ & \times \operatorname{sech}^2 \left(\frac{\beta E_{\mathbf{k},\sigma\mu}}{2} \right) + \left(\frac{\epsilon_{\mathbf{k}}}{E_{\mathbf{k},\sigma\mu}} \partial_i \partial_j \epsilon_{\mathbf{k}} \right. \\ & \left. \left. + \frac{\Delta_{c\mathbf{k}}}{E_{\mathbf{k},\sigma\mu}} \partial_i \partial_j \Delta_{c\mathbf{k}} \right) \frac{\sigma\mu + E_{\mathbf{k}}^*}{E_{\mathbf{k}}^*} \tanh \left(\frac{\beta E_{\mathbf{k},\sigma\mu}}{2} \right) \right\}, \quad (67) \end{aligned}$$

where $E_{\mathbf{k}}^* = \sqrt{\epsilon_{\mathbf{k}}^2 + \Delta_{c\mathbf{k}}^2}$ and

$$E_{\mathbf{k},\sigma\mu} = [(\sqrt{\epsilon_{\mathbf{k}}^2 + \Delta_{c\mathbf{k}}^2} + \sigma\mu)^2 + \Delta_s^2]^{1/2}$$

is the generalized dispersion in the extended CDW band.

The nonlocal properties valid in the $q \rightarrow 0$ limit do not depend on the details of the cutoff Λ . For this reason, we are allowed to take Λ to infinity with no further consequences. However, the Green functions method leads to some spurious results in the ultraviolet if we do not take the Brillouin zone into account. To see this, consider the illustrative case of the normal CDW band Hamiltonian (65). After a suitable diagonalization into a particle-hole eigenstate basis with eigenvalues $\pm E_{\mathbf{k}}^* = \pm \sqrt{\epsilon_{\mathbf{k}}^2 + \Delta_{c\mathbf{k}}^2}$, we may write it into the form

$$H_{\text{CDW}} = \sum_{\mathbf{k}} E_{\mathbf{k}}^* \bar{\Psi}^\dagger(\tilde{\mathbf{k}}) \eta_3 \bar{\Psi}(\tilde{\mathbf{k}}).$$

The London kernel of this problem can be derived directly from Eq. (66) by setting $\Delta_s = \mu = 0$, ignoring the $\Delta_{c\mathbf{k}}$ terms on it, and performing the substitution $\epsilon_{\mathbf{k}} \rightarrow E_{\mathbf{k}}^*$. It is immediate to see that in this case one has

$$Q_{ij}^{\text{CDW}} = A_j \sum_{\mathbf{k}} \partial_i \left[(\partial_j E_{\mathbf{k}}^*) \tanh \left(\frac{\beta E_{\mathbf{k}}^*}{2} \right) \right]$$

resulting in a nonzero surface term for $i=j$, which diverges in the ultraviolet for any monotonically crescent $E_{\mathbf{k}}^*$. The integrability of the results derived by this method depends on the introduction of states in the entire Brillouin zone. In particular, we have that $\langle j_i^{\text{CDW}} \rangle = 0$ (as expected) by assuming that the surface term cancels in the Brillouin zone because of its periodicity. In order to fix the spurious divergences, we adopt an argument due to Lifshitz and Pitaevskii.⁴⁴ Considering that the kernel for $\Delta_s = 0$ is zero, since no supercurrents are induced by the magnetic field, there is no physical result in subtracting the normal phase kernel from the SC kernel

$$\langle j_i \rangle = [Q_{ij}(\Delta_s) - Q_{ij}(0)] A_j. \quad (68)$$

We may consider that the kernel above correctly incorporates the Brillouin zone effects, at least near the phase transition.

To analyze the spectral weight behavior due to the Meissner effect within the cone approximation $\epsilon_{\mathbf{k}} \sim v_F k_{\perp}$ and $\Delta_{c\mathbf{k}}$

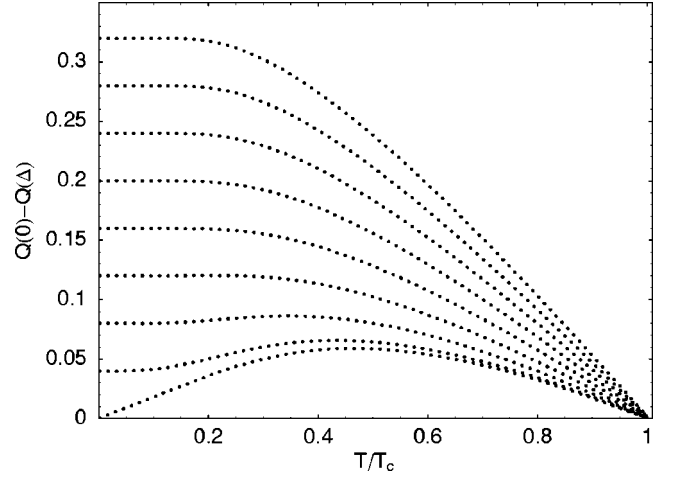


FIG. 16. London kernel dependence with temperature in the cone approximation ($g/g_c = 1.1$). Plots for $0 \leq |\mu|/\alpha \leq 0.16$, from the bottom to the top, in fixed intervals of 0.02. $Q(0) - Q(\Delta_s)$ in units of $e^2 v_F \alpha / (2\pi d v_{\Delta c})$.

$\sim v_{\Delta} k_{\parallel}$, we calculate the London equation in two limits, near the normal-SC transition and at $T=0$. Including the Brillouin zone $[-\pi/d, \pi/d]$ in the normal direction to the planes, with d the interplane distance, from Eq. (66), we have

$$Q_{\perp}(\Delta_s) = v_F^2 \frac{\beta e^2}{2c} \sum_{\mathbf{k}, \sigma=\pm 1} \operatorname{sech}^2 \left(\frac{\beta E_{\mathbf{k},\sigma\mu}}{2} \right).$$

At $T=0$, the kernel gives

$$Q_{\perp}(\Delta_s) - Q_{\perp}(0) \xrightarrow{T \rightarrow 0} - \frac{|\mu| e^2 v_F}{d \pi v_{\Delta c}}$$

confirming the anomalous behavior detected by the f -sum rule (51) in the optical conductivity.

In the opposite limit, for $T \sim T_c$, the kernel in the strong coupling approximation ($\beta_c |\mu| \ll 1$) gives

$$\begin{aligned} Q_{\perp}(\Delta_s) - Q_{\perp}(0) \\ \xrightarrow{T \rightarrow T_c} - \frac{\beta_c v_F e^2}{4d \pi v_{\Delta c}} \left(1 + \mu^2 \frac{\beta_c}{4} \right) \Delta_s^2, \end{aligned}$$

in agreement with the mean-field result for the penetration depth $\lambda_{\perp} = \sqrt{c / \{4\pi [Q_{\perp}(0) - Q_{\perp}(\Delta_s)]\}} \propto \Delta_s^{-1}$.

The dependence of the London kernel with μ and the temperature is shown in Fig. 16. There is a clear suppression of the Meissner effect in the low-temperature region, especially when the density of states in the Fermi surface nodes is close to zero. As we discussed previously in Sec. VI, the opening of a SC gap in a nodal liquid possibly causes the spectral shift of high-energy states beyond the cone cutoff α in the CDW band to the infrared. As we mentioned before, the spectral shift of the states below α (~ 60 meV) has actually been observed in the normal CDW phase of the TaSe₂ crystal.²² More experimental studies are required to understand the SC phase properties in this crystal.

VIII. DISCUSSIONS

In this paper we have studied the thermodynamic and transport properties of a model proposed originally in Ref. ²⁴ for the coexistence of a gapless CDW phase and an s -wave superconductor in TMD. While the lattice inversion symmetry is broken in the CDW distorted phase, as observed experimentally by neutron diffraction, we propose a pairing ansatz which also violates the time-reversal symmetry. According to the ansatz, the pairing of the electrons is mediated by virtual acoustic phonons via a piezoelectric coupling, and the center-of-mass momentum of the pairs equals the CDW wave vectors connecting different sheets of the TMD Fermi surface. This additional broken symmetry has dramatic consequences on the spin-exchange interaction and produces an anisotropic NMR response along the normal direction to the triple-CDW plane. In contrast to TaSe₂, the quasiparticles of NbSe₂ are well defined in the Fermi-liquid regime. The SC phase of NbSe₂ has been extensively studied and indicates that a conventional BCS description is warranted.^{34–36}

In contrast to the BCS theory, which is not critical, the gap equation (13) has a QCP in the critical coupling $g=g_c$ when the system exhibits particle-hole symmetry ($\mu=0$). When this symmetry is broken, the SC gap Δ_s is strongly rescaled by μ as the coupling parameter is modified, and the QCP is suppressed. The scaling of the quantity Δ_s/μ follows two different coupling regimes: (i) “Fermi-liquid” sector in weak coupling, for $g < g_c$, where Δ_s/μ flows to zero as $g \rightarrow 0$ and (ii) strong-coupling marginal limit for $g > g_c$, where $\Delta_s/|\mu| \gg 1$. The specific-heat jump is strongly attenuated in the particle-hole symmetric case (where $\Delta C_V/C_n=0.35$), because of the low density of states at the Fermi energy. As expected, in the Fermi-liquid regime we recover the jump of the BCS model $\Delta C_V/C_n=1.43$.

We have observed several anomalous properties in the transport. Unlike traditional one-band superconductors, the spectra for optical and thermal conductivities in the clean limit have an infrared peak due to the thermal channels of quasiparticle excitation. These channels involve thermal intraband excitations, promoting the electrons in the condensate to the empty states of the pocket, at the top of the lower band (see Fig. 13). The absorption window for this channel is limited to the pocket energy $2|\mu|$. A second kind of absorption channel is due to interband excitations, when a pair is broken as a result of the absorption of a photon. In this case, the electron is excited to the upper band, across the optical gap barrier $\omega_0=2\sqrt{\mu^2+\Delta_s^2}$. The later type depends on the number of electrons in the condensate and is more effective at $T=0$, except for a few channels at a given frequency ω_a which are abruptly suppressed by the temperature reduction (say, below T_a) because of the optical gap enlargement, that is $\omega_a < \omega_0(T)$ for $T < T_a$. The thermal channels on the contrary vanish at $T=0$ with no exception.

The optical conductivity has an absorption edge at ω_0 . The coherence factors are affected by the broken lattice inversion symmetry in the CDW phase. The f -sum rule reveals an anomalous suppression of the diamagnetic spectral weight, mainly for $\mu=0$. This behavior is an evidence that there are missing high-energy diamagnetic states in the SC

phase, which would be attracted from the bottom to the top of the lower band by the opening of the SC gap in TaSe₂. Close to the normal-SC phase transition, however, these states can be introduced by the same procedure that fixes the anomalous divergence of the London kernel in the ultraviolet, which is due to the absence of the Brillouin zone periodicity into the calculation. We have extended the calculation to a general CDW band where the loss of the crystal inversion symmetry is included by assumption.

In summary, we have presented a complete theory for s -wave superconductivity in nodal liquids. We have calculated the thermodynamics, various response functions, and transport properties of this system and have shown that these quantities deviate strongly from the same properties in ordinary BCS superconductors. We believe our theory can be applied to some TMD, such as 2H-TaSe₂ or 2H-TaS₂, and our predictions can be checked experimentally.

ACKNOWLEDGMENTS

B. U. and G. G. C. are indebted to E. Miranda for many helpful discussions. B. U. acknowledges FAPESP (Fundação de amparo à pesquisa do Estado de São Paulo), Project No. 00/06881-9, for the financial support. A.H.C.N. was partially supported through NSF Grant No. DMR-0343790.

APPENDIX A: GAP EQUATION

In this appendix we derive Eqs. (21)–(23). Applying the variable substitution $\nu=v_F\bar{k}+\sigma\mu$, the equation (13) can be written into the form

$$\begin{aligned}
 1 &= \frac{g v_F}{4 \pi v_{\Delta} \sigma_{\pm 1}} \sum \int_0^{s_{\sigma}} d\bar{k} \frac{\bar{k}}{E_{\mathbf{k}, \sigma \mu}} \tanh\left(\beta \frac{E_{\mathbf{k}, \sigma \mu}}{2}\right) \\
 &= \frac{g}{4 \pi v_{\Delta} v_F} \left\{ \frac{4}{\beta} \ln[\cosh(\beta \alpha / 2) \operatorname{sech}(\beta \sqrt{\Delta_s^2 + \mu^2} / 2)] \right. \\
 &\quad \left. + \mu \int_{-\mu}^{\mu} d\nu \frac{1}{\sqrt{\nu^2 + \Delta_s^2}} \tanh\left(\frac{\beta}{2} \sqrt{\nu^2 + \Delta_s^2}\right) \right\}. \quad (\text{A1})
 \end{aligned}$$

In the $|\mu|/\Delta_s \ll 1$ limit we find:

$$1 = \frac{g}{4 \pi v_{\Delta} v_F} \left\{ \frac{4}{\beta} \ln \left[\frac{\cosh(\beta \alpha / 2)}{\cosh(\beta \Delta_s / 2)} \right] + \frac{\mu^2}{\Delta_s} \tanh\left(\frac{\beta}{2} \Delta_s\right) \right\},$$

which is equivalent to Eq. (21). We notice, however, that the above expression remains valid at T_c (i.e., for finite μ and $\Delta_s \rightarrow 0$) if the strong-coupling approximation $|\mu|/\Delta_{0\mu} \ll 1$ is satisfied.

We define $\alpha=2\pi v_F v_{\Delta}/g_c$. Close to T_c , taking $\Delta_s \rightarrow 0$, we obtain

$$\frac{2g_c}{g} = \frac{4}{\beta_c \alpha} \ln \left[\cosh\left(\frac{\beta_c \alpha}{2}\right) \right] + \frac{\mu^2 \beta_c}{2\alpha}.$$

The critical temperature for $g > g_c$ is

$$T_c = \frac{1}{2k_B \ln 4} \left[\Delta_0 + \sqrt{\Delta_0^2 + \mu^2 \ln 4} \right], \quad (\text{A2})$$

where $\Delta_0 \equiv \Delta_s(T=0, g, \mu=0) = \alpha(1-g_c/g)$. The expression that gives the critical dependence of the gap with tempera-

ture for $(|\mu|/\Delta_{0\mu} \gg 1)$ follows directly from the expansion of the gap equation (13) in terms of $\beta\Delta_s$.

To calculate the critical temperature in the weak-coupling regime, we take $\Delta_s \rightarrow 0$ in Eq. (A1), giving

$$\frac{2g_c}{g} = \frac{4}{\beta_c \alpha} \ln \left[\frac{\cosh(\beta_c \alpha/2)}{\cosh(\beta_c \mu/2)} \right] + \frac{2|\mu|}{\alpha} \left[\ln \left(\frac{\beta_c |\mu|}{2} \right) \times \tanh \left(\frac{\beta_c |\mu|}{2} \right) - \int_0^{\beta_c |\mu|/2} d\zeta \frac{\ln \zeta}{\cosh^2 \zeta} \right]$$

after integrating the second term of Eq. (A1) by parts. If $\beta_c |\mu| \geq 4$, the integration above can be extended to the interval $[0, \infty]$,

$$\frac{2g_c}{g} = 2 + \frac{2|\mu|}{\alpha} \left[\ln \left(\frac{\beta_c |\mu| \gamma}{\pi} \right) - 1 \right].$$

In weak coupling $(|\mu|/\Delta_{0\mu} \gg 1)$ the condition $\beta_c |\mu| \gg 1$ is easily satisfied. The equation above implies that

$$T_c = \frac{|\mu| \gamma}{k_B \pi} e^{\alpha(1-g_c/g)|\mu|^{-1-1}}, \quad (\text{A3})$$

where $\ln \gamma \cong 0.577$ is the Euler constant.

In the weak-coupling regime, we can find the gap equation near the phase transition. For $\beta|\mu| \gg 1$, we use the power series expansion in $\beta\Delta_s \ll 1$ of the integral⁴⁵

$$\int_0^\mu dv \frac{\tanh \left(\frac{\beta}{2} \sqrt{v^2 + \Delta_s^2} \right)}{\sqrt{v^2 + \Delta_s^2}} \sim \int_0^\mu dv \frac{1}{v} \tanh \left(\frac{\beta}{2} v \right) - \frac{7\zeta(3)}{8} \frac{\beta^2 \Delta_s^2}{\pi^2}.$$

Expanding the gap equation (A1) in lowest order around β_c , we find

$$\Delta_s(T \rightarrow T_c, \mu) \xrightarrow{\beta_c \mu \gg 1} \frac{1}{\beta_c} \left[\frac{7\zeta(3)}{8\pi^2} + \frac{1}{2\beta_c^2 \mu^2} \right]^{-1/2} \sqrt{\frac{T_c - T}{T_c}}. \quad (\text{A4})$$

The weak-coupling expansions above are correct whenever $\tanh(\beta_c |\mu|/2) \sim 1$ or $\beta_c |\mu| \geq 4$.

APPENDIX B: SPECIFIC HEAT

In this section we calculate explicitly the specific heat jump in the weak and strong coupling limits. The entropy of the problem is given by

$$S = -k_B \sum_{\mathbf{k}, \gamma, \sigma} [(1 - n_{\mathbf{k}, \sigma \mu}^\gamma) \ln(1 - n_{\mathbf{k}, \sigma \mu}^\gamma) + n_{\mathbf{k}, \sigma \mu}^\gamma \ln n_{\mathbf{k}, \sigma \mu}^\gamma],$$

where $n_{\mathbf{k}, \sigma \mu}^\gamma = (e^{\gamma \beta E_{\mathbf{k}, \sigma \mu}} + 1)^{-1}$ is the Fermi-Dirac distribution, indexed by $\sigma = \pm 1$, and by the two branches of the cone $\gamma = \pm 1$. The specific heat yields³³

$$C_V = -\beta \frac{dS}{d\beta} = -k_B \beta \sum_{\mathbf{k}, \alpha, \sigma} \gamma \frac{\partial n_{\mathbf{k}, \sigma \mu}^\gamma}{\partial E_{\mathbf{k}, \sigma \mu}} \left(E_{\mathbf{k}, \sigma \mu}^2 + \frac{\beta}{2} \frac{d\Delta_s^2}{d\beta} \right). \quad (\text{B1})$$

At the phase transition, the specific-heat jump reads

$$\begin{aligned} \Delta C(\beta_c, \mu) &= \lim_{\beta \rightarrow \beta_c} \left[-k_B \frac{\beta_c^2}{2} \frac{d\Delta_s^2}{d\beta} \sum_{\mathbf{k}, \gamma, \sigma} \gamma \frac{\partial n_{\mathbf{k}, \sigma \mu}^\gamma}{\partial E_{\mathbf{k}, \sigma \mu}} \right] \\ &= \frac{k_B \beta_c^3}{8\pi v_\Delta v_F} \frac{d\Delta_s^2}{d\beta} \Big|_{\beta_c} \\ &\times \sum_{\sigma=\pm 1} \int_0^\alpha d\epsilon \epsilon \operatorname{sech}^2 \left(\frac{\beta_c(\epsilon + \sigma\mu)}{2} \right). \end{aligned}$$

If $\beta_c \alpha \geq 4$, we may extend the integration range to infinity. This integral can be evaluated in two limits, for $\beta_c |\mu| \ll 1$ and $\beta_c |\mu| \gg 1$, which yields

$$\begin{aligned} \Delta C(\beta, \mu) &\rightarrow \frac{k_B \beta_c}{2\pi v_\Delta v_F} \frac{d\Delta_s^2}{d\beta} \Big|_{\beta_c} \\ &\times \begin{cases} \ln 4 + \frac{\beta_c^2 \mu^2}{4}, & \text{for } \beta_c |\mu| \ll 1, \\ \beta_c |\mu|, & \text{for } \beta_c |\mu| \gg 1. \end{cases} \quad (\text{B2}) \end{aligned}$$

From Eqs. (22) and (A2), we find:

$$\frac{d\Delta_s^2}{d\beta} \Big|_{\beta_c} = \begin{cases} \frac{4}{\beta_c^2} \left(\ln 4 + \frac{\beta_c \mu^2}{4} \right), & \text{for } \beta_c |\mu| \ll 1, \\ \frac{1}{\beta_c^3} \left(\frac{7\zeta(3)}{8\pi^2} + \frac{1}{2\beta_c^2 \mu^2} \right)^{-1}, & \text{for } \beta_c |\mu| \gg 1. \end{cases} \quad (\text{B3})$$

In the normal phase, the specific heat C_{Vn} is obtained from Eq. (B1),

$$\begin{aligned} C_{Vn}(\beta_c) &= \frac{k_B \beta_c^2}{4\pi v_\Delta v_F} \sum_{\sigma=\pm 1} \int_0^\alpha d\epsilon \epsilon (\epsilon + \sigma\mu)^2 \\ &\times \operatorname{sech}^2 \left(\frac{\beta_c(\epsilon + \sigma\mu)}{2} \right). \end{aligned}$$

Evaluating the integral gives:

$$C_{Vn}(\beta_c) \rightarrow \frac{k_B}{2\pi v_F v_\Delta \beta_c^2} \begin{cases} 18\zeta(3), & |\mu| \beta_c \ll 1, \\ \frac{2}{3} \pi^2 \beta_c |\mu|, & |\mu| \beta_c \gg 1. \end{cases} \quad (\text{B4})$$

Combining Eqs. (B2)–(B4), we find

$$\frac{\Delta C_V}{C_{n,V}} \Big|_{T_c} = \begin{cases} \frac{2 \ln 4}{9\zeta(3)} \left(\ln 4 + \frac{\beta_c^2 \mu^2}{2} \right), & |\mu| \beta_c \ll 1, \\ \frac{3}{2\pi^2} \frac{1}{\frac{7\zeta(3)}{8\pi^2} + \frac{1}{2\beta_c^2 \mu^2}}, & |\mu| \beta_c \gg 1. \end{cases} \quad (\text{B5})$$

APPENDIX C: CORRELATION FUNCTIONS

We define the charge and spin susceptibilities from the imaginary time ordered correlation functions:

$$\chi^c(\mathbf{q}, i\omega) = - \int_0^\beta d\tau e^{i\omega\tau} \langle T_\tau [\rho(\mathbf{q}, \tau) \rho(-\mathbf{q}, 0)] \rangle, \quad (\text{C1})$$

$$\chi_{ab}^s(\mathbf{q}, i\omega) = - \int_0^\beta d\tau e^{i\omega\tau} \langle T_\tau [S_a(\mathbf{q}, \tau) S_b(-\mathbf{q}, 0)] \rangle, \quad (\text{C2})$$

with ρ and S_a , respectively, the charge- and spin-density operators defined by Eqs. (29) and (34).

The optical, thermal, and thermoelectric correlation functions are defined as

$$\Pi_{ij}(\mathbf{q}, i\omega) = - \int_0^\beta d\tau e^{i\omega\tau} \langle j_i(\mathbf{q}, \tau) j_j(-\mathbf{q}, 0) \rangle, \quad (\text{C3})$$

$$\Pi_{ij}^{EE}(\mathbf{q}, i\omega) = - \int_0^\beta d\tau e^{i\omega\tau} \langle j_i^E(\mathbf{q}, \tau) j_j^E(-\mathbf{q}, 0) \rangle, \quad (\text{C4})$$

$$\Pi_{ij}^E(\mathbf{q}, i\omega) = - \int_0^\beta d\tau e^{i\omega\tau} \langle j_i^E(\mathbf{q}, \tau) j_j(-\mathbf{q}, 0) \rangle, \quad (\text{C5})$$

where j is the electric current operator (44) and j^E is the thermal current operator defined by Eq. (54).

APPENDIX D: HAMILTONIAN IN THE BALIAN-WERTHAMER SPACE

In this Appendix we discuss Eq. (35). The BW space is introduced to extend the pairs space ($\mathbf{k}\uparrow, -\mathbf{k}\downarrow$) to a larger one where the spin and momentum degrees of freedom are decoupled. The procedure rests on ‘‘duplicating’’ the Hamiltonian (keeping it invariant by summing in half Brillouin zone), interchange the order of the ψ fermionic operators in the duplicated term, and explore the symmetry under the $\mathbf{k} \rightarrow -\mathbf{k}$ exchange in the k sum. The CDW Hamiltonian in the BW space reads

$$\begin{aligned} H_{\text{CDW}} &= \sum_{\mathbf{k}, \sigma, a, b} v_F \psi_{a\sigma}^\dagger(\mathbf{k}) \bar{\mathbf{k}} \cdot \tilde{\eta}^{ab} \psi_{b\sigma}(\mathbf{k}) \\ &= \frac{v_F}{2} \sum_{\mathbf{k}, a, b} \bar{\mathbf{k}} \cdot [\psi_{a\uparrow}^\dagger(\mathbf{k}) \tilde{\eta}^{ab} \psi_{b\uparrow}(\mathbf{k}) + \psi_{a\downarrow}^\dagger(\mathbf{k}) \tilde{\eta}^{ab} \psi_{b\downarrow}(\mathbf{k}) \\ &\quad + \psi_{b\uparrow}^\dagger(-\mathbf{k}) \tilde{\eta}^{ba} \psi_{a\uparrow}^\dagger(-\mathbf{k}) + \psi_{b\downarrow}^\dagger(-\mathbf{k}) \tilde{\eta}^{ba} \psi_{a\downarrow}^\dagger(-\mathbf{k})] \\ &= \sum_{\mathbf{k} \in \frac{1}{2}\text{BZ}} v_F \Psi^\dagger(\mathbf{k}) \sigma_0 \tau_0 \tilde{\eta} \cdot \bar{\mathbf{k}} \Psi(\mathbf{k}) \end{aligned} \quad (\text{D1})$$

by the definition of the BW spinor (33).

The chemical potential term (6) can also be written as $-\mu \sum_{\mathbf{k} \in \frac{1}{2}\text{BZ}} \Psi^\dagger(\mathbf{k}) \sigma_0 \tau_3 \eta_0 \Psi(\mathbf{k})$. The pairing term can be obtained with the use of the antisymmetric property of the Pauli matrix η_2 under the transposition $\eta_2^{ab} \rightarrow -\eta_2^{ba}$, namely,

$$\begin{aligned} H_P &= \sum_{\mathbf{k}, a, b} \Delta_s \psi_{a\uparrow}^\dagger(\mathbf{k}) \eta_2^{ab} \psi_{b\downarrow}^\dagger(-\mathbf{k}) + \text{H.c.} \\ &= \frac{1}{2} \sum_{\mathbf{k}, a, b} \Delta_s [\psi_{a\uparrow}^\dagger(\mathbf{k}) \eta_2^{ab} \psi_{b\downarrow}^\dagger(-\mathbf{k}) + \psi_{a\downarrow}^\dagger(-\mathbf{k}) \eta_2^{ab} \psi_{b\uparrow}(\mathbf{k}) \\ &\quad + \psi_{b\downarrow}^\dagger(\mathbf{k}) \eta_2^{ba} \psi_{a\uparrow}^\dagger(-\mathbf{k})] + \psi_{b\uparrow}(-\mathbf{k}) \eta_2^{ba} \psi_{a\downarrow}(\mathbf{k}) \\ &= - \sum_{\mathbf{k} \in \frac{1}{2}\text{BZ}} \Delta_s \Psi^\dagger(\mathbf{k}) \sigma_3 \tau_1 \eta_2 \Psi(\mathbf{k}). \end{aligned} \quad (\text{D2})$$

APPENDIX E: LONDON KERNEL

In this appendix, we calculate the London kernel (66). It can be derived from the calculation of the expectation value of the current density operator

$$\begin{aligned} \langle \vec{j}_i \rangle(\mathbf{k}) &= \text{Tr} \sum_{\mathbf{k}} \left[e \left(\partial_i \epsilon_{\mathbf{k}} - \frac{e}{c} A^j \partial_i \partial_j \epsilon_{\mathbf{k}} \right) \langle \Psi^\dagger(\tilde{\mathbf{k}}) \tau_0 \eta_3 \Psi(\tilde{\mathbf{k}}) \rangle \right. \\ &\quad \left. + e \left(\partial_i \Delta_{c\mathbf{k}} - \frac{e}{c} A^j \partial_i \partial_j \Delta_{c\mathbf{k}} \right) \langle \Psi^\dagger(\tilde{\mathbf{k}}) \tau_0 \eta_1 \Psi(\tilde{\mathbf{k}}) \rangle \right] \end{aligned} \quad (\text{E1})$$

at first order in \mathbf{A} , where in our definition $\tilde{\mathbf{k}} = \mathbf{k} - (e/c)\tau_3\mathbf{A}$. Expanding the Green function $\vec{G}(i\omega_n, \tilde{\mathbf{k}}) = (i\omega_n - \tilde{\omega}_{\tilde{\mathbf{k}}})^{-1}$ up to leading order,

$$\begin{aligned} &\text{Tr} \langle \Psi^\dagger(\tilde{\mathbf{k}}) \tau_\mu \eta_\nu \Psi(\tilde{\mathbf{k}}) \rangle \\ &= \frac{1}{\beta} \text{Tr} \sum_{\omega_n} \tau_\mu \eta_\nu \vec{G}_0 \left[1 - \frac{e}{c} \vec{G}_0 (\partial_i \epsilon_{\mathbf{k}} \tau_0 \eta_3 + \partial_i \Delta_{c\mathbf{k}} \tau_0 \eta_1) A_i \right], \end{aligned}$$

where \vec{G}_0 is the Green function (12). The zeroth order terms are:

$$\begin{aligned} &\text{Tr} \langle \Psi^\dagger(\tilde{\mathbf{k}}) \tau_0 \eta_3 \Psi(\tilde{\mathbf{k}}) \rangle_0 \\ &= \frac{1}{\beta} \text{Tr} \sum_{\omega_n} \tau_0 \eta_3 \vec{G}_0 \\ &= \epsilon_{\mathbf{k}} \sum_{\sigma=\pm 1} \frac{\mu\sigma + E_{\mathbf{k}}^*}{E_{\mathbf{k}}^* E_{\mathbf{k}, \sigma\mu}} [n(E_{\mathbf{k}, \sigma\mu}) - n(-E_{\mathbf{k}, \sigma\mu})] \end{aligned} \quad (\text{E2})$$

and

$$\begin{aligned} &\text{Tr} \langle \Psi^\dagger(\tilde{\mathbf{k}}) \tau_0 \eta_1 \Psi(\tilde{\mathbf{k}}) \rangle_0 \\ &= \Delta_{c\mathbf{k}} \sum_{\sigma=\pm 1} \frac{\mu\sigma + E_{\mathbf{k}}^*}{E_{\mathbf{k}}^* E_{\mathbf{k}, \sigma\mu}} [n(E_{\mathbf{k}, \sigma\mu}) - n(-E_{\mathbf{k}, \sigma\mu})], \end{aligned} \quad (\text{E3})$$

where $E_{\mathbf{k}}^* \equiv \sqrt{\epsilon_{\mathbf{k}}^2 + \Delta_{c\mathbf{k}}^2}$ and

$$E_{\mathbf{k},\sigma\mu} = [(E_{\mathbf{k}}^* + \sigma\mu)^2 + \Delta_s^2]^{1/2}.$$

At first order, we find after a straightforward calculation

$$\begin{aligned} & \text{Tr}\langle\Psi^\dagger(\tilde{\mathbf{k}})\tau_0\eta_3\Psi(\tilde{\mathbf{k}})\rangle_1 \\ &= -\frac{e}{c}A_i\partial_i\epsilon_{\mathbf{k}}\frac{1}{\beta}\sum_{\omega_n}\text{Tr}[(\vec{G}_0)^2] \\ &= -\frac{e}{c}\sum_{\sigma=\pm 1}A^i(\partial_i\epsilon_{\mathbf{k}})\frac{\partial}{\partial E_{\sigma\mu}}[n(E_{\sigma\mu}) - n(-E_{\sigma\mu})] \quad (\text{E4}) \end{aligned}$$

and

$$\begin{aligned} \text{Tr}\langle\Psi^\dagger(\tilde{\mathbf{k}})\tau_0\eta_1\Psi(\tilde{\mathbf{k}})\rangle_1 &= -\frac{e}{c}\sum_{\sigma=\pm 1}A^i(\partial_i\Delta_{c\mathbf{k}}) \\ &\times\frac{\partial}{\partial E_{\sigma\mu}}[n(E_{\sigma\mu}) - n(-E_{\sigma\mu})]. \end{aligned} \quad (\text{E5})$$

The London kernel (66) follows from the direct substitution of Eqs. (E2)–(E5) into Eq. (E1), just noting that the zero order current term

$$\begin{aligned} \langle j \rangle_0 &= \sum_{\sigma=\pm 1} \sum_{\mathbf{k}} e(\epsilon_{\mathbf{k}}\partial_i\epsilon_{\mathbf{k}} + \Delta_{c\mathbf{k}}\partial_i\Delta_{c\mathbf{k}}) \frac{\mu\sigma + E_{\mathbf{k}}^*}{E_{\mathbf{k}}^*E_{\mathbf{k},\sigma\mu}} \\ &\times [n(E_{\mathbf{k},\sigma\mu}) - n(-E_{\mathbf{k},\sigma\mu})] \end{aligned}$$

is zero by symmetry when integrated in k .

-
- ¹R. L. Withers and J. A. Wilson, *J. Phys. C* **19**, 4809 (1986).
²J. A. Wilson and A. D. Yoffe, *Adv. Phys.* **18**, 193 (1969); J. A. Wilson, F. J. DiSalvo, and S. Mahajan, *Adv. Phys.* **24**, 117 (1975).
³J. P. Tidman, O. Singh, and A. E. Curzon, *Philos. Mag.* **30**, 1191 (1974).
⁴D. A. Whitney, R. M. Fleming, and R. V. Coleman, *Phys. Rev. B* **15**, 3405 (1977).
⁵R. M. Fleming, D. E. Moncton, D. B. McWhan, and F. J. DiSalvo, *Phys. Rev. Lett.* **45**, 576 (1980).
⁶D. B. McWhan, J. D. Axe, and R. Youngblood, *Phys. Rev. B* **24**, 5391 (1981).
⁷T. Valla, A. V. Fedorov, P. D. Johnson, J. Xue, K. E. Smith, and F. J. DiSalvo, *Phys. Rev. Lett.* **85**, 4759 (2000).
⁸R. A. Klemm, *Physica C* **341**, 839 (2000).
⁹C. W. Chu, V. Diatschenko, C. Y. Huang, and F. J. DiSalvo, *Phys. Rev. B* **15**, 1340 (1977).
¹⁰G. Wexler and A. M. Wooley, *J. Phys. C* **9**, 1185 (1976).
¹¹J. A. Wilson, *Phys. Rev. B* **15**, 5748 (1977).
¹²D. E. Moncton, J. D. Axe, and F. J. DiSalvo, *Phys. Rev. B* **16**, 801 (1977).
¹³W. Sacks, D. Roditchev, and J. Klein, *Appl. Phys. A: Mater. Sci. Process.* **66**, 925 (1998).
¹⁴Th. Straub, Th. Finteis, R. Claessen, P. Steiner, S. Hufner, P. Blaha, C. S. Oglesby, and E. Bucher, *Phys. Rev. Lett.* **82**, 4504 (1999).
¹⁵W. C. Tonjes, V. A. Greanya, Rong Liu, C. G. Olson, and P. Molinie, *Phys. Rev. B* **63**, 235101 (2001).
¹⁶T. M. Rice and G. M. Scott, *Phys. Rev. Lett.* **35**, 120 (1975); L. VanHove, *Phys. Rev.* **89**, 1189 (1953).
¹⁷K. Rossnagel, O. Seifarth, L. Kipp, M. Skibowski, D. Voss, P. Kruger, A. Mazur, and J. Pollmann, *Phys. Rev. B* **64**, 235119 (2001).
¹⁸O. Seifarth, S. Gliemann, M. Skibowski, and L. Kipp, *J. Electron Spectrosc. Relat. Phenom.* **137**, 675 (2004).
¹⁹Rong Liu, C. G. Olson, W. C. Tonjes, and R. F. Frindt, *Phys. Rev. Lett.* **80**, 5762 (1998).
²⁰C. Wang, B. Giambattista, C. G. Slough, R. V. Coleman, and M. A. Subramanian, *Phys. Rev. B* **42**, 8890 (1990).
²¹T. Valla, A. V. Fedorov, P. D. Johnson, P.-A. Glans, C. McGuinness, K. E. Smith, E. Y. Andrei, and H. Berger, *Phys. Rev. Lett.* **92**, 086401 (2004).
²²V. Vescoli, L. Degiorgi, H. Berger, and L. Forro, *Phys. Rev. Lett.* **81**, 453 (1998).
²³P. B. Littlewood and C. M. Varma, *Phys. Rev. B* **46**, 405 (1992); C. M. Varma, P. B. Littlewood, S. Schmitt-Rink, E. Abrahams, and A. E. Ruckenstein, *Phys. Rev. Lett.* **63**, 1996 (1989); **64**, 497 (1990).
²⁴A. H. Castro Neto, *Phys. Rev. Lett.* **86**, 4382 (2001).
²⁵M. Vojta, Y. Zhang, and S. Sachdev, *Phys. Rev. B* **62**, 6721 (2000).
²⁶C. M. Varma and W. Weber, *Phys. Rev. Lett.* **39**, 1094 (1977).
²⁷D. P. DiVincenzo and E. J. Mele, *Phys. Rev. B* **29**, 1685 (1984); J. Gonzalez, F. Guinea, and M. A. H. Vozmediano, *Phys. Rev. Lett.* **77**, 3589 (1996).
²⁸D. Pines and J. R. Schrieffer, *Nuovo Cimento* **X**, 496 (1958).
²⁹B. Uchoa, A. H. Castro Neto, and G. G. Cabrera, *Phys. Rev. B* **69**, 144512 (2004).
³⁰P. W. Anderson, *J. Phys. Chem. Solids* **11**, 46 (1959).
³¹P. W. Anderson, *Phys. Rev. B* **30**, 4000 (1984).
³²L. N. Cooper, *Phys. Rev.* **104**, 1189 (1956).
³³M. Tinkham, *Introduction to Superconductivity* (McGraw-Hill, New York, 1996).
³⁴R. A. Craven and S. F. Meyer, *Phys. Rev. B* **16**, 4583 (1977).
³⁵P. Garoche, J. J. Veyssié, P. Manuel, and P. Moliné, *Solid State Commun.* **19**, 455 (1976); R. E. Schwall, G. R. Stewart, and T. H. Geballe, *J. Low Temp. Phys.* **22**, 557 (1976).
³⁶N. Kobayashi, K. Noto, and Y. Muto, *J. Low Temp. Phys.* **27**, 217 (1977); D. Sanchez, A. Junod, J. Muller, H. Berger, and F. Lévy, *Physica B* **204**, 167 (1995).
³⁷S. V. Dordevic, D. N. Basov, R. C. Dynes, B. Ruzicla, V. Vescoli, L. Degiorgi, H. Berger, R. Gaál, L. Forró, and E. Bucher, *Eur. Phys. J. B* **33**, 15 (2003).
³⁸J. R. Schrieffer, *Theory of Superconductivity* (Benjamin, New York, 1964).
³⁹G. D. Mahan, *Many-particle Physics* (Plenum, New York, 1981).

⁴⁰R. Balian and N. R. Werthamer, Phys. Rev. **131**, 1553 (1963).

⁴¹X. Yang and C. Nayak, Phys. Rev. B **65**, 064523 (2002).

⁴²R. D. Parks, *Superconductivity* (Marcel Dekker, New York, 1969), Vol. 1, Chap. 2.

⁴³M. E. Peskin and D. V. Schroeder, *An Introduction to Quantum Field Theory* (Addison Wesley, Reading, MA, 1995), p. 18.

⁴⁴E. M. Lifshitz and L. P. Pitaevskii, *Statistical Physics* (Pergamon, Oxford, 1980), Vol. 2, p. 213.

⁴⁵A. A. Abrikosov, L. P. Gorkov, and I. E. Dzyaloshinski, *Methods of Quantum Field Theory in Statistical Physics* (Prentice Hall, New Jersey, 1964), p. 304.